Investigating Preservation of Stable Isotope Ratios in Subfossil Deep-Sea Proteinaceous Coral Skeletons as Paleo-Recorders of Biogeochemical Information over Multimillennial Timescales

Danielle S. Glynn, UC Santa Cruz, CA, USA. Corresponding Author Email: dglynn@ucsc.edu

Kelton McMahon, University of Rhode Island, RI, USA. Email: kelton_mcmahon@uri.edu

Owen Sherwood, Dalhousie University, Halifax, NS, Canada. Email: owen.sherwood@dal.ca

Thomas P. Guilderson, UC Santa Cruz, CA, USA. Email: tguilder@ucsc.edu

Matthew D. McCarthy, UC Santa Cruz, CA, USA. Email: mdmccar@ucsc.edu

Abstract:

Paleoproxy records in deep-sea proteinaceous coral skeletons can reconstruct past ocean conditions on centennial to millennial time scales. Commonly recovered subfossil specimens could potentially extend these archives through the Holocene. However, protein matrix stability and integrity of stable isotope proxies over multi-millennial timescales in such specimens have never been examined. Here we compare amino acid (AA) composition together with bulk and AA compound-specific carbon ($\delta^{13}C$) and nitrogen ($\delta^{15}N$) isotopes in live-collected and subfossil (~9.6-11.6 kyrs BP) *Kulamanamana haumeaae* deep-sea coral specimens from the central Pacific to understand the effects of long-duration benthic oxic exposure on primary coral chemistry. We find large coupled shifts in bulk $\delta^{15}N$ (~7‰) and $\delta^{13}C$ (~2‰) in the outermost portion (0-10 mm) of the subfossil coral, coincident with extensive alteration of the protein matrix. Microstructural changes in skeletal texture coincide with higher C/N ratios (+0.8) and isotope-based amino acid degradation parameters (e.g. $\Sigma V \geq 3$), indicating extensive degradation of seawater-exposed gorgonin. However, interior gorgonin (>10 mm) retained amino acid molecular compositions (with exception of major Glycine loss) and bulk and amino acid-specific isotopic values that were similar to live-collected specimens. These results indicate that compound-specific isotope analysis of amino acids can reconstruct paleo-oceanographic biogeochemical and ecosystem information in subfossil corals beyond a clear diagenetic horizon, which is easily identifiable from an evaluation of C/N ratios together with the ΣV degradation proxy.

1. Introduction

Deep-sea proteinaceous corals are ideal recorders of sub-decadal resolution surface biogeochemistry, due to their ubiquitous distribution, long lifespans, and near continuous deposition of skeletal material (reviewed in Williams 2020). These corals consume organic matter exported from the surface ocean and incorporate the isotopic values of exported production into concentric growth layers in their proteinaceous skeletons (Druffel et al., 1995; Roark et al., 2006). In recent years, deep-sea proteinaceous coral skeletons have been used to reconstruct the history of exported organic matter over centennial to millennial timescales globally, including the North Pacific Gyre (Sherwood et al., 2014; McMahon et al., 2015; Glynn et al., 2019), North Atlantic (Sherwood et al. 2009a, 2011), southern Australia (Sherwood et al., 2009b), the Equatorial Pacific (Williams and Grottoli, 2010), and the California Margin (Hill et al., 2014; Schiff et al., 2014). Deep-sea proteinaceous coral studies have been particularly useful in understanding the most recent millennia of ocean history, a period characterized by rapid oceanographic and climatic change, but one in which detailed sedimentary records in many locations are severely limited by slow sedimentation rates or significant bioturbation. In many regions, proteinaceous corals also represent the only archive capable of decadal or finer temporal scale reconstructions, making them especially useful to understand multi-decadal variability of biogeochemical cycling and phytoplankton community dynamics recorded in the signal of export production (Sherwood et al., 2011; 2014, McMahon et al., 2015).

To properly evaluate paleo-environmental interpretations from organic proxies, the preservation of chemical and isotopic information must be carefully considered. Proteinaceous deep-sea coral skeletons are composed of a cross-linked, fibrillar protein that is among the most diagenetically resistant proteinaceous materials known (Goldberg, 1974, 1976; Ehrlich, 2010;

53 Strzepek et al., 2014). For example, skeletons of black corals are predominantly composed of
54 protein (~50-70%) and contain lipids, diphenols, and chitin (Holl et al. 1992). However, far less
55 is known for gold corals besides being composed of primarily amino acids (AAs) (Goodfriend
56 1997, Sherwood et al. 2006, 2014). At the molecular level, the AA composition of modern *K.*
57 *haumeaae* shows little variability over the duration of the coral skeleton's growth (Goodfriend,
58 1997; Sherwood et al., 2006), and AA composition is also similar in live-collected versus 1000-
59 2000 year old specimens (Sherwood et al., 2006), suggesting that coral skeleton protein is stable
60 over at least millennial time frames.

61 The abundance of non-living coral skeletons encountered on the seafloor in many
62 locations suggests the possibility to go far beyond the time horizon constrained by living corals.
63 For example, Guilderson and coauthors (2013) describe a range of ^{14}C dated specimens from
64 both the Hawaiian and Line Islands that collectively spanned the entire Holocene. Edinger and
65 Sherwood (2012) conducted year-long decay experiments on deep-sea corals of different skeletal
66 compositions and documented a range of physical changes such as pitting, corrosion, hydration,
67 and disintegration of the organic gorgonin. Noé and Dullo (2006) and Noé et al. (2007) noted the
68 presence of micritized borings in subfossil gorgonian corals. To date, there have been no detailed
69 studies of $\delta^{15}N$ and $\delta^{13}C$ preservation of subfossil deep-sea proteinaceous coral specimens
70 collected in-situ on the seafloor. Thus, the susceptibility of the gorgonin protein matrix to
71 degradation and the integrity of archived geochemical information on multi-millennial timescales
72 are not well known. A detailed understanding of skeletal preservation over long timescales will
73 substantially improve confidence in the use of subfossil corals for paleoceanographic study,
74 since degradative effects could easily be confused with signatures of past environmental
75 variation.

The goal of this study was to assess the integrity of the $\delta^{15}N$ and $\delta^{13}C$ values and AA profiles recorded in deep-sea proteinaceous corals over extensive time and degradation potential. We compared the structural, chemical, and isotopic data in a subfossil (~9.6-11.6 kyr BP) coral with the same properties in a live-collected specimen from the same location at Cross Seamount, Hawaii. We used a multi-metric approach to examine central aspects of physical, chemical, and isotopic change as a function of preservation along a gradient from inner protected layers to outer seawater exposed regions. Scanning electron microscopy (SEM) was used to investigate physical structural change in the skeleton matrix. Chemical composition changes were examined using bulk tissue carbon to nitrogen (C/N) elemental ratios and molecular-level AA composition (mol%). Patterns in bulk tissue $\delta^{15}N$ and $\delta^{13}C$ values as well as carbon and nitrogen compound-specific isotope analysis of AAs (CSIA-AA) were compared to examine potential impacts of degradation on geochemical fidelity. These comparisons allowed us to directly determine how ~10 kyrs of oxic seawater exposure altered the chemistry and the paleo-archival potential of the proteinaceous skeleton. We used these data to propose metrics for evaluating the integrity of proteinaceous corals and the geochemical data they archive.

2. Materials and Methods

2.1 Study site and sample collection

Living and subfossil deep-sea proteinaceous corals (*Kulamanamana haumaeae*) were collected from 447 and 415 m respectively from Cross Seamount (19°N, 158°W), southwest of the Big Island of Hawaii, in 2004. Cross Seamount waters at 400 m have average in situ temperatures of ~9 °C and dissolved oxygen concentration of ~100-120 μmol/kg (Boyer et al., 2018). The polyps of live-collected corals were removed and all skeletons were rinsed first with seawater, followed by freshwater, before being air dried on deck. In the lab, ~0.7 cm thick cross-

99 sectional disks were sectioned from near the base of each skeleton, then polished and mounted to
100 glass slides, following standard procedures (Sherwood et al., 2014). A detailed sample
101 processing flow chart and description can be found in the supplemental file (Fig. S1A).

102 **2.2 Scanning electron microscopy (SEM)**

103 For scanning electron microscope images, sections of the same coral disks were coated
104 with ~20 nm of gold using a Technics Hummer VI sputter coater (3 minutes @ 80 mtorr, 17 mA
105 current) and then imaged on a FEI Quanta 3D dual beam microscope (electron beam operating at
106 5 kV and 6.7 pA) in the W.M. Keck Center for Nanoscale Optofluidics at the University of
107 California – Santa Cruz. SEM images (300 µm and 30-40 µm resolution) were visually
108 compared to examine structural changes in the skeletal matrix between the live-collected and
109 subfossil corals.

110 **2.3 Radiocarbon dating and age models**

111 Radiocarbon dating was performed on nine sample aliquots (~1 mg total material) each
112 spread ~5 mm apart along the skeleton cross section transect. Samples were first fumed with
113 concentrated HCl and subsequently dried before being transferred with methanol into 6 mm short
114 quartz tubes and dried. The 6 mm tubes were then placed inside larger 9 mm quartz tubes with an
115 appropriate amount of CuO, prior to pumping off excess atmosphere, sealing, and combusting to
116 produce CO_2. The CO_2 after cryogenic purification was converted to graphite and analyzed at the
117 Lawrence Livermore National Laboratory. Results were corrected for $\delta^{13}C$ and background ^{14}C
118 using similarly handled ^{14}C-free coal. Radiocarbon results were transformed into calibrated years
119 before present (yr BP). These ages and subsequent age models were generated with Calib 8.2
120 (Stuiver et al. 2021) using a local reservoir (ΔR) correction of -177 ± 16, (Druffel et al., 2001;

121 Guilderson et al., 2021) and the Marine20 database (Heaton et al. 2020) and linearly interpreted
122 to provide a continuous age-model.

123 **2.4 Bulk stable isotope analysis**

124 A computerized Merchanteck micromill was used to drill a radial transect from the
125 outside to the inner layers of the coral skeleton cross section at 0.1 mm resolution, yielding 2-3
126 mg of powdered skeletal material per sample interval. All 168 samples from the live-collected
127 coral were analyzed (155 samples in duplicate); while of the 455 subfossil samples drilled, 193
128 were analyzed, with a greater sample density analyzed from the outermost 10 mm. Bulk
129 powdered coral material (~0.4 mg) was enclosed in tin capsules for bulk $\delta^{13}C$ and $\delta^{15}N$ analyses
130 via continuous-flow isotope-ratio mass spectrometry (IRMS) using a Carlo-Erba elemental
131 analyzer connected to an Optima Isotope Ratio Mass Spectrometer (IRMS). C/N ratios were
132 simultaneously determined. The analytical error for these measurements, as determined from
133 analysis of standards of known composition (pugel and acetanilide), was ±0.2‰ for both $\delta^{13}C$
134 and $\delta^{15}N$ values and ±0.1 for C/N ratios. To test for the impact of secondary authigenic carbonate
135 in the sample matrix, a subset of the same samples from the subfossil coral (1–2 mg each, n = 7)
136 were acidified using 1 N HCl for 20 h under refrigerated conditions, followed by filtration onto a
137 0.22 μm glass fiber filter. The filter was dried overnight at 45°C before material was transferred
138 into a tin capsule and analyzed following the same procedure as described above.

139 **2.5 Amino Acid Molar Percent**

140 Adjacent growth bands were combined to obtain ~10-11 mg of total material which, after
141 homogenization, was used for each analysis (typically used 8-10 samples of ~1 mg from each
142 adjacent 0.1 mm layers). Of these composite samples, approximately 0.5-1 mg of coral material
143 was needed for measurement of AA molar concentrations, with the rest being used for CSIA-AA

144 described in Section 2.6. Wet chemical protocols for AA measurements in proteinaceous corals
145 followed established protocols (detailed in McMahon et al, 2018). Briefly, individual AAs were
146 liberated using standard acid hydrolysis conditions (1 ml of 6 N HCl at 110°C for 20 h), then
147 spiked with a norleucine internal standard and derivitized, followed by purification with cation-
148 exchange chromatography and a salt-removal step (p-buffer = KH_2PO_4 + Na_2HPO_4 in Milli-Q
149 water, pH 7), and finally rinsed with chloroform three times with centrifugation before final
150 conversion to trifluoroacetyl/isopropyl ester (TFAA) derivatives. The AA mole percent (mol%)
151 compositions were quantified using a GC–MS (Agilent 7890 GC coupled to a 5975 MSD) based
152 on single ion monitoring data of the major ion relative to authentic AA external standard
153 calibration curves. Commercial AA standards (Pierce Biochemicals) were used to create
154 concentration series, and response factors from these external standards were used to calculate
155 relative molar concentrations. Reproducibility, as measured by the standard deviation of GC-MS
156 replicates analyses, typically averaged <5 mol%.

157 **2.6 Compound Specific Stable Isotope Analysis of Amino Acids (CSIA-AA)**

158 CSIA-AA for both carbon and nitrogen was performed on aliquots of the same TFAA
159 derivatives prepared as described in Section 2.5, using ~4 mg for $\delta^{13}C$ and ~6 mg $\delta^{15}N$ CSIA-AA
160 measurements. Derivatized samples were injected in triplicate on a coupled Gas
161 Chromatography- IRMS (Thermo Trace GC, coupled to a Delta + IRMS), as described in
162 McMahon et al. (2018). Isotopic ratios were measured for 13 of the common protein AAs (see
163 supplementary material, Fig. S1): alanine (Ala), glycine (Gly), serine (Ser), valine (Val),
164 threonine (Thr), leucine (Leu), isoleucine (Ile), proline (Pro), phenylalanine (Phe), tyrosine
165 (Tyr), lysine (Lys), glutamine + glutamic acid (Glx), and asparagine + aspartic acid (Asx).
166 Cystine (Cys) and histidine (His) break down during acid hydrolysis and were not measured.

For $\delta^{13}C_{AA}$ higher sensitivity coupled with good chromatographic separation permitted all AA $\delta^{13}C$ values to be measured in single chromatographic run (Fig. S1). However for $\delta^{15}N_{AA}$, the much larger on-column AA amounts required by much lower intrinsic IRMS sensitivity for N made it impossible to obtain both adequate chromatography and peaks sizes simultaneously for all AAs in a single run. We therefore performed independent GC-IRMS $\delta^{15}N$ run series for high verses low mol% AAs (Fig. S1). The early eluting AA peaks (Ala, Gly, Ser, Thr, and Val) were all large and well separated (Fig. S1) and necessitated only duplicate injections. GC-IRMS error was therefore reported for these peaks as mean deviations. Subsequent independent runs at higher concentrations then employed a cut-off method to remove early peaks (directed to back-flush), so that lower mol% peaks could be quantified (Asx, Glx, Ile, Leu, Lys, Phe, Pro, Tyr). These injections were made in triplicate, with concentrations adjusted to produce at least 80 mV IRMS N_2 signal intensity for the smallest peaks (typically Phe and Ile).

Overall reproducibility for individual AA isotopes values among sample injections was, in general, <1‰ for both $\delta^{13}C$ and $\delta^{15}N$ CSIA-AA, based on internal lab working standards. Accuracy of $\delta^{13}C$ and $\delta^{15}N$ CSIA-AA data was verified following protocols described in McCarthy et al., 2013. Briefly, three independent, overlapping approaches were used to assess accuracy: first a Nor-Leu internal standard added to every sample, second an external (L-amino acid) AA standard mix injected repeatedly after every third sample, and finally a natural cyanobacteria long term (> 10 yr) in-house working standard, run as an unknown with every sample batch. The Nor-Leu internal standard was used to verify that each specific injection for each sample gave expected values. The external bracketed standards were used in different ways for $\delta^{13}C$ and $\delta^{15}N$ values based on the need to correct for added derivatization moieties for $\delta^{13}C$ only. For $\delta^{13}C$, the measured IRMS values are not actual AA $\delta^{13}C$ values but must corrected for

added derivative C; this was done following the method of Silfer (1991). For $\delta^{15}N$ values the measured IRMS values directly represent the $\delta^{15}N$ value of each AA and therefore external standard values can be used to directly assess accuracy and make corrections. For $\delta^{15}N$, the average measured $\delta^{15}N$ value of each external standard AA across the entire run was therefore compared against its authentic value, and any systematic bias/offset used to correct sample AA values, following the approach described by McCarthy et al., 2013 (supplementary information, Fig. S2). Finally, both $\delta^{13}C$ and $\delta^{15}N$ AA results from the McCarthy lab internal laboratory reference material (dried/homogenized cyanobacteria) standard run with each sample batch were evaluated for accuracy against a long term (>10 yr) internal control chart. The supplemental file contains more information on the order of sample processing, including specific protocols for CSIA-AA corrections, representative chromatograms, and minimum mV peak information (Fig. S1A, S1B).

2.7 Nomenclature, AA groupings, and CSIA-AA parameters

We report and discuss AA isotope data in terms of commonly used CSIA-AA groupings for both $\delta^{13}C$ and $\delta^{15}N$, which in turn are based on metabolic pathways and observed differences in isotope fractionation during trophic transfer (reviewed by McMahon and McCarthy, 2016, Ohkouchi et al., 2017). For $\delta^{15}N$ data, we treat Phe, Tyr, and Lys as Source AAs (those with minimal isotope fractionation during trophic transfer); Asx, Glx, Ile, Leu, Pro, Val as Trophic AAs (close linkage to central glutamate pool, with correspondingly large isotope fractionation during trophic transfer), and Gly and Ser as Intermediate AAs, based on recent literature that shows they display variable behavior, very often falling between the two customary groupings (McMahon and McCarthy, 2016). Lastly, Thr was plotted alone, as it displays a unique inverse isotope fractionation behavior with trophic transfer (McMahon and McCarthy, 2016).

For $\delta^{13}C$, we used common essential and non-essential AAs categories. There is minimal isotope fractionation for essential AAs with trophic transfer, while there can be highly variable fractionation in the nonessential AAs due to resynthesis (McMahon et al. 2010). The essential AAs (Thr, Ile, Val, Phe, and Leu) can be synthesized by both phytoplankton and microbes, however most metazoans cannot synthesize them and must incorporate the essential AA from their diet (Larsen et al. 2013). While we note that it is possible that some coral species, or more likely microbes associated with them, could also potentially synthesize essential AA, prior work has indicated that essential AA $\delta^{13}C$ CSIA-AA in proteinaceous corals correspond to expected primary production patterns and local endmember values and thus directly track export production (Schiff et al., 2014, McMahon et al., 2018, Shen et al., 2021).

We quantified possible microbial reworking of skeletal protein using AA $\delta^{15}N$ values using the CSIA-AA metric $\sum V$, which is a proxy for total heterotrophic microbial AA resynthesis of proteinaceous material (McCarthy et al., 2007, Ohkouchi et al, 2017). $\sum V$ was calculated using the average deviation of $\delta^{15}N$ values of the trophic AAs Ala, Val, Leu, Ile, Pro, Asx, Glx:

$$\sum V = \frac{1}{n}\sum |X_i|$$

where X_i is the offset in $\delta^{15}N$ of each individual AA from the average ($X_i = \delta^{15}N_i - \text{AVG } \delta^{15}N_i$), and n is the number of AAs used in the calculation.

The CSIA-AA-based trophic position ($TP_{\text{CSIA-AA Skeleton}}$) of deep-sea corals is a proxy for trophic structure of both the coral and the overlying planktonic food web contributing to export production. This parameter was calculated using the difference in Phe (source) and Glx (trophic) $\delta^{15}N$ values according to a proteinaceous coral – specific formula:

235 $$TP_{CSIA-AA\ Skeleton} = 1 + \left(\frac{\delta^{15}N_{Glx} + \partial - \delta^{15}N_{Phe} - \beta}{TDF_{Glx-Phe}}\right)$$

236 recently determined by McMahon et al. (2018). This formula incorporates an additional
237 correction factor (∂) for Glx of 3.4 ± 0.1‰ to account for the consistent offsets observed between
238 polyp and skeletal Glx $\delta^{15}N$ values across multiple deep-sea coral species (McMahon et al.,
239 2018). The β value (3.4‰; empirical difference between the $\delta^{15}N_{Glx}$ and $\delta^{15}N_{Phe}$ of non-vascular
240 autotrophs) and the TDF value (7.6‰; trophic discrimination factor of $\delta^{15}N_{Glx}$ relative to $\delta^{15}N_{Phe}$
241 per trophic transfer; Chikaraishi et al., 2009). We note that alternate β (3.3 ± 1.8‰; Ramirez et
242 al. 2021) and TDF (6.6 ± 1.7‰; Nielson et al. 2015) values have recently been proposed to
243 represent better averages over many ecosystems. We present alternate TP value using these
244 values in the supplemental material, however because the lower TDF value in particular gives
245 unrealistically high TP values for corals, we have here elected to use the same β and TDF values
246 used for deep sea proteinaceous corals in McMahon et al. (2018).

247 **2.8 Statistics and interpretational framework**

248 We discuss coral data in the context of different regions of degradation, described by
249 ranges of radial distance along the skeletal disc. The subfossil coral is discussed mainly in terms
250 of three separate zones for bulk isotopic and C/N data: 1) outer diagenetic horizon (0-10 mm), as
251 defined by very rapid changes in both C/N and isotope values, 2) inner, intermediate zone (10-36
252 mm) defined by only minor offsets from expected values, and 3) the innermost most protected
253 zone (>36 mm), with C/N values within expected ranges for live-collected specimens. However,
254 for the mol% and CSIA-AA data these changes are only observed in the outermost layer. We
255 therefore discuss these results only for the two distinct zones: 1) the outer diagenetic horizon (0-
256 5 mm) and 2) the inner layers from 10 mm to the skeleton's center. For data from a live-collected

coral there are no analogous degradation zones, however, here we group results to separate pre-industrial samples from the Industrial Revolution, using 1900 CE based on coral-specific age models as a comparison of data more comparable to the subfossil coral.

For CSIA-AA comparisons between live and subfossil specimens and within the subfossil coral (0-5 mm versus >10 mm), the AA isotope data were normalized by taking each individual AA isotope value and subtracting the average value of all total hydrolysable AAs (THAA) in that sample, to allow direct examination of biosynthetic patterns (after McCarthy et al., 2007) without the confounding variable of differential $\delta^{15}N$ baseline. The normalized data include propagation of errors in quadrature. We note that for THAA normalized values the errors become larger because of the spread in AA values from which the average THAA value is calculated and the process of data normalization. This is important information for understanding that the uncertainty in these types of calculations is not unduly biased by small n in this case. To test for significant differences across zones, measured parameters were compared using two-sample group t-tests, assuming unequal variances with 95% confidence intervals. Statistics were calculated using Real Statistics Resource Pack software (Release 6.2; Zaiontz, 2019).

3. Results

The live-collected specimen had a radius of 17 mm and radiocarbon analyses (n = 11) indicated an age of ~710 years (research data 1). The subfossil specimen had a radius of 46 mm and radiocarbon analyses (n = 9) indicated an age of 1,890 yrs (~9,670 to 11,560 years BP; Fig. S2, research data 2).

3.1 Scanning Electron Microscopy

Under 125x magnification, the live-collected coral skeleton exhibited concentric growth layers, exaggerated by the presence of desiccation cracks generated during sample drying,

aligned parallel to the growth layers (Fig. 1A). Under 1250x magnification, the live-collected coral growth layers were imaged as <1 μm thick sheets of tightly woven fibers (Fig. 1B). For the subfossil coral, the outer skeleton appeared less dense (Fig. 1C) and exhibited a flakey microstructure with an absence of the tightly woven fibers (Fig. 1D). The inner section of the same subfossil coral appeared less altered compared to the outer skeleton and retained a concentrically layered appearance (Fig. 1E) along with some of the woven fibrous character, despite the presence of flakey microstructure (Fig 1F).

3.2 C/N ratios

The C/N values from all subsamples of the live-collected modern coral averaged 2.75 ± 0.11 and were invariant within the analytical error. C/N values were higher in the subfossil specimen, increasing from 3.12 ± 0.05 (n = 18) in the innermost skeleton, to 3.28 ± 0.12 (n = 88) in the middle 10-36 mm zone of the skeleton, to 3.36 ± 0.16 (n = 88) in the outer 10 mm of the skeleton. Acidification resulted in small decreases of 0.09-0.14 in C/N ratios compared to non-acidified samples for the intermediate and innermost layers, which was within instrumental error of the non-acidified sample C/N ratios, and more substantial decreases of 0.32–0.68 in C/N ratios compared to non-acidified samples in the outer 10 mm (n = 3, research data 3 and 4).

The mean elemental weight percent of subfossil samples for the outermost layer (0-10 mm) was 4.7 ± 0.9 wt% C and 15.7 ± 2.6 wt% N (n = 88), with a low value of 2.9 wt% C and 10.7 wt% N observed in the outermost 0.1 mm. The inner intermediate zone (10-36 mm, n = 88) mean elemental weight percent was 5.4 ± 0.8 wt% C and 17.6 ± 2.4 wt% N with no clear trend. The innermost zone (>36 mm, n = 18) mean was 7.0 ± 0.7 wt% C and 21.8 ± 2.1 wt% N (research data 4), falling within the range of modern specimens.

3.3 AA Molar Distribution

The modern coral AA mol% values (Fig. 3, research data 5) for all AAs recovered were consistent with previous results for AA composition of *K. haumaeea* gorgonin (Druffel et al. 1995; Goodfriend, 1997; Sherwood et al. 2014). However, for the subfossil coral the mol% value of Gly alone was much lower (29.0 ± 3.8%) than observed in the modern coral (52.4 ± 2.4%; Fig. 3B). When Gly was removed from the relative mol% calculation then the mol% distribution of remaining AA was essentially identical between subfossil and modern corals (research data 7.3) with only the mol% values for Ser, Val, Pro, and Thr showing small, but significantly different values between the subfossil (>10 mm) and live-collected coral ($p = <0.002$, research data 7).

Within the subfossil coral zones there were no significant differences in relative mol% for Ala, Thr, Ser, Val, Leu, Ile, Pro, and Phe between the inner (>10 mm) and outer (0-5 mm) layers (research data 7). Five other AAs did have small but statistically significant changes in mol% from the inner (>10 mm) to outer (0-5 mm) layers (Fig. 3A): decreases in Tyr (-3.2%, $p = 0.023$), Lys (-3.9%, $p = 0.001$), and increases in Asp (+1.9%, $p = 0.008$), Gly (+3.7%, $p = 0.02$), and Glu (+0.9%, $p = 0.06$).

3.4 Bulk $\delta^{15}N$ and $\delta^{13}C$ Results

Bulk $\delta^{15}N$ values in the Cross Seamount live-collected coral were 11.2 ± 0.5‰ (n = 290) before the Industrial Revolution (1270-1900 C.E.) with a high of 12.5‰ in ~1410 C.E. During the 1900's Industrial Revolution the $\delta^{15}N$ values declined steadily to a low value of ~8.8‰ in the outermost layers (research data 3). Mean bulk $\delta^{13}C$ values in the live-collected coral skeleton from the preindustrial era (prior to 1900 C.E.) were -16.3 ± 0.3‰ (n = 290), reaching a high of -

15.5‰ during the 1620-1650s C.E. Similar to bulk $\delta^{15}N$ values, $\delta^{13}C$ values also declined after the 1900s to the lowest observed value of -17.2‰ in the outermost layers (research data 3).

Subfossil coral skeleton $\delta^{15}N$ values were overall more positive than the live-collected coral, ranging from 12 to 20‰ (research data 4). Within the subfossil coral the outermost $\delta^{15}N$ values (0-10 mm) increased by ~7‰ relative to the mean to a high of ~20.1‰ in the outer ~1 mm, while the intermediate region (10-36 mm) mean value was 13.7 ± 0.5‰ with no temporal trend (n = 88; Fig. 2B). The innermost zone (>36 mm) mean $\delta^{15}N$ value was (12.6 ± 0.6‰; n = 18) and was slightly lower relative to the intermediate zone (Fig. 2B).

The bulk $\delta^{13}C$ values in the subfossil coral ranged from -17.3 to -14.6‰ over the entire record (Fig. 2C), very similar to the modern coral from this site as well as to other coral records reported from the North Pacific Subtropical Gyre region (McMahon et al., 2015). Similar to the $\delta^{15}N$ data, there was a large (~2‰) and nearly monotonic increase in $\delta^{13}C$ values in the outer layers (0-10 mm) of the skeleton. The intermediate region (10-36 mm) mean value was -16.5 ± 0.4‰ (n = 88) and the innermost (>36 mm) mean value was -17.0 ± 0.3‰ (n = 18). Similar to C/N results discussed in Section 3.2, acidification prior to EA analysis reduced $\delta^{13}C$ values primarily in the outer 0-10 mm layers (0.6-1.4‰ lower relative to unacidified skeleton; n = 3) and to a lesser extent in intermediate region (10-36 mm; 0.4-0.9‰ lower relative to unacidified skeleton; n = 3). There were no significant differences in $\delta^{13}C$ values due to acidification observed in the innermost zone (>36 mm) (Fig. 2C, research data 4.2). While these results suggest progressive influence of authigenic calcite, under a microscope there were no visible formation of bubbles when raw coral material was subjected to 1 N HCl at room temperature.

3.5 CSIA-AA $\delta^{13}C$ data

The normalized $\delta^{13}C$ CSIA-AA values ($\delta^{13}C_{norm\text{-}AA}$) showed very similar biosynthetic patterns between the modern specimen and the inner subfossil coral layers (>10 mm, Fig. 4). Within the subfossil coral, $\delta^{13}C_{norm\text{-}AA}$ values also remained similar between the subfossil's inner (>10 mm) and outer (0-5 mm) regions (Fig. 4), in contrast to the large changes observed in $\delta^{15}N_{norm\text{-}AA}$ values in the outermost horizon (Fig. 5). Comparing the normalized patterns of the pre-industrial live-collected (n = 3) and subfossil (inner >10 mm, n = 6) corals only two non-essential AAs had statistically different $\delta^{13}C_{norm\text{-}AA}$ values (Asp -2.3‰, p = 0.01, Pro +1.4‰, p = 0.03). The mean essential AA $\delta^{13}C_{EAA}$ values (Phe, Thr, Ile, Leu, Val, Lys) of deep-sea corals have been shown to directly reflect $\delta^{13}C$ baseline of export production (Schiff et al., 2014, Shen et al. 2021). The live-collected Cross Seamount coral (excluding the rapidly shifting regions after the Industrial Revolution) had a mean essential $\delta^{13}C_{EAA}$ value of -18.6 ± 0.3‰ (n = 3, research data 11). The subfossil Cross Seamount inner layers $\delta^{13}C_{EAA}$ values (-16.0 ± 1.5‰; n = 6, research data 12) were +2.6‰ more positive than the modern specimen from the same location (Fig. 6). The subfossil coral's outer layers (0-5 mm) had a mean $\delta^{13}C_{EAA}$ value of -17.1 ± 0.7‰ (n = 2, research data 12), and there were no significant differences in $\delta^{13}C_{EAA}$ values between the normalized outer (0-5 mm, n = 2) and inner (>10 mm, n = 6) subfossil coral zones (Fig. 4, research data 13).

3.6 CSIA-AA $\delta^{15}N$ data

Normalized CSIA-AA $\delta^{15}N$ patterns ($\delta^{15}N_{norm\text{-}AA}$) were very similar between the subfossil coral inner (>10 mm) layers and modern coral (Fig. 5, research data 8 and 9), consistent with the similarity observed in AA molar composition (with the sole exception of Gly).

368 Comparing $\delta^{15}N_{norm\text{-}AA}$ values between the subfossil inner layers (>10 mm, n = 6; Fig. 5; blue
369 filled circles) and the pre-industrial live-collected (n = 3; Fig. 5; yellow filled circles) coral, all
370 $\delta^{15}N_{norm\text{-}AA}$ values except for Glx and Ile fell within one standard deviation of modern coral data.
371 Gly and Ile had clear offsets from modern coral $\delta^{15}N_{norm\text{-}AA}$ patterns (Glx +3.4‰, p = 4.6E-5 and
372 Ile -7.2‰, p = 0.002). Four additional AAs also had smaller offsets between modern and
373 subfossil (>10 mm) coral $\delta^{15}N_{norm\text{-}AA}$ values, which while statistically significant for these runs,
374 were also not notably different from typical analytical variation for GC-IRMS analyses (Asx
375 +1.7‰, p = 0.02, Ser +2.1‰, p = 0.02, Lys +2.5‰, p = 0.004, and Phe +1.5‰, p = 0.02;
376 research data 10). A sample $\delta^{15}N$ CSIA-AA chromatograph showing peak separation for both
377 modern and subfossil coral hydrolysate is in the supplemental material (Fig. S1B). Mean THAA
378 $\delta^{15}N_{norm\text{-}AA}$ values were 17.7 ± 1.0‰ (n = 5) for the outer diagenetic horizon (0-5 mm), while the
379 inner layers (>10 mm) mean THAA $\delta^{15}N_{norm\text{-}AA}$ values were 19.2 ± 0.8‰ (n = 6). This offset in
380 THAA $\delta^{15}N_{norm\text{-}AA}$ values was in the opposite direction of the bulk $\delta^{15}N$ trend (Fig. 6).

381 In contrast to the similar and very consistent CSIA-AA patterns observed in the inner >10
382 mm layers described above, the $\delta^{15}N_{norm\text{-}AA}$ values in the outer seawater exposed layers were
383 highly variable, with some more positive (Asx, Lys, Gly, Ala, Val, Ser, Leu; Fig. S3), others
384 more negative (Ile, Thr, Glx, Pro; Fig. S4), and some varying with no consistency across
385 subsamples analyzed (Phe, Tyr; Fig. S5). After normalization to THAA (proxy for average
386 protein $\delta^{15}N$ value) there were also significant differences in $\delta^{15}N_{norm\text{-}AA}$ patterns between the
387 outer diagenetic horizon (0-5 mm, n = 5) and inner layers (>10 mm, n = 6) (Fig. 5; red vs. yellow
388 filled circles). These normalized values, reflecting the relative biosynthetic offset from average
389 protein, were substantially different for most AAs: Asx (+2.3‰, p = 0.01), Gly (+2.1‰, p =

390 0.006), Lys (+1.8‰, p = 0.02), Ala (+2.8‰, p = 0.03), Val (+3.0‰, p = 0.03), Pro (+2.4‰, p =
391 0.03), and Thr (-14.5‰, p = 0.01; Fig. 5, research data 10).

392 **3.7 Trophic and Degradation Proxies**

393 Consistent with the individual AA isotope differences presented in Section 3.5, there
394 were very large differences in the ∑V parameter for microbial degradation and protein
395 resynthesis between modern and subfossil corals, in particular between the inner verses outer
396 zones of the subfossil specimen. Due to the uniquely large $\delta^{15}N$ offset of Ile (-7.2‰) between
397 live-collected and subfossil specimens, ∑V was calculated both with and without Ile. The
398 modern specimen had very consistent standard ∑V values, mean 2.7 ± 0.1 (3.0 ± 0.2 when Ile
399 was excluded, n = 4, Fig. 6C). The subfossil inner (>10 mm) layers, where most $\delta^{15}N_{AA}$ data
400 were consistent with live-collected coral, also had a consistent but elevated standard ∑V value of
401 4.0 ± 0.3 using all AA (n=6). However, this result was very strongly driven by Ile $\delta^{15}N$ values
402 alone. Recalculating ∑V without Ile, the inner subfossil coral average ∑V was 3.4 ± 0.2 (n = 6),
403 comparable to data for the modern coral. Finally, the diagenetic horizon (0-5 mm) subfossil coral
404 layers had very high ∑V values, reaching among the highest values (range 5-6, Fig. 6C, research
405 data 9).

406 $TP_{CSIA\text{-}AA\ Skeleton}$ values also varied substantially within the subfossil coral but were again
407 similar between the inner subfossil layers (>10 mm) and the modern coral. Subfossil inner layers
408 (>10 mm) had $TP_{CSIA\text{-}AA\ Skeleton}$ values with a mean of 3.1 ± 0.1 (n = 5), very close to modern
409 coral values (3.3 ± 0.5, n = 4), while the subfossil outer layers reached a low $TP_{CSIA\text{-}AA\ Skeleton}$ of
410 1.2 (at 2.8 mm) in the same region with highest ∑V (Fig. 6D). Alternative calculations for
411 trophic position were also examined, all indicating similar trends within and among zones (Fig.
412 S6).

4. Discussion

Understanding the long-term preservation of deep-sea proteinaceous coral skeletons is critical to extending the time horizon of paleo-applications using these valuable bioarchives. Comparisons of subfossil (~9.6-11.6 kyr BP) and modern *K. haumeaae* skeletons across a wide range of physical features, bulk chemical composition based on C/N, bulk $\delta^{13}C$ and $\delta^{15}N$ values, molecular level AA molar percentages and isotope compositions, and CSIA-AA parameters for degradation (ΣV) and trophic position (TP_{CSIA}) show excellent preservation of physical and geochemical composition in the inner subfossil coral skeleton. These findings lend confidence to the paleo-application of geochemical proxies in deep-sea proteinaceous coral skeletons to reconstruct biogeochemical cycling, plankton community trophic dynamics, and export production back through the Holocene. At the same time, we also clearly identified a very distinct seawater exposed, outer diagenetic horizon of the skeleton with both abiotic alteration (e.g., loss of glycine, potential carbonate addition) and biotic degradation (e.g., increased variability in AA isotope values, ΣV, $TP_{CSIA\text{-}AA\ Skeleton}$) accompanied by physical changes in the skeleton matrix (SEM images). Identification of this region will help to avoid potential misinterpretation of geochemical data in degraded regions of these archives.

4.1 Physical structure: matrix changes in subfossil coral

Skeletons of *K. haumeaae* exhibit concentric growth layers composed of a tightly bound fibrillar protein, similar to other proteinaceous corals (Goldberg, 1976; Noé and Dullo 2006; Sherwood et al. 2006). Visually there was little difference in skeletons between the live-collected and subfossil specimens without magnification. While the subfossil disk was lighter in color, with a drier, flaky outer crust, there was no visual indication of the physical or chemical

435 degradation zonation. Specifically, the diagenetic horizon (outer 10 mm) discussed extensively
436 in subsequent subsections, could not be visually identified.

437 Under higher magnification (SEM) structural differences between the live-collected and
438 subfossil specimens were readily apparent (Fig. 1). For the live-collected specimen the regular
439 banded fibrous layers were clearly visible in SEM images (Fig. 1A, 1B). This suggests while the
440 modern skeleton itself is not living, it was physically very well protected from the influence of
441 ocean water by the living outer polyp colony and intact outer skeleton. It has been hypothesized
442 that the tightly woven fibrous structure of proteinaceous coral skeletons contributes to
443 degradation resistance by preventing seawater penetration (Druffel et al., 1995), with the
444 implication being that physical protection slows down biological as well as abiotic compositional
445 changes. Similar physical protection of organic matter is well known in a range of matrixes
446 including as eggshell/bone (e.g., Hendy, 2021) and soil organic matter (e.g., Krull et al., 2003).
447 In shallow water carbonate corals it is only after the polyps die that the skeleton is exposed and
448 significant colonization by bacteria, borers, and physical grazing occurs (Le Campion-Alsumard
449 et al. 1995). The protection of the inner coral skeleton is therefore likely applicable to other
450 genera of corals as well as skeletons of different ages but further research is necessary to confirm
451 this.

452 The subfossil coral skeleton showed hallmarks of matrix degradation at both a macro and
453 microscale level, particularly in the outer most, seawater exposed zone of the skeleton (Fig.1).
454 Visually, a more brittle and paper-like apparent character in SEM images of the very outermost
455 layers (<0.1 mm) suggest possible structural changes in the protein matrix. Furthermore, SEM
456 imaging showed clear loss of tightly woven fibers and a flakey microstructure (Fig 1C, 1D).
457 Overall, the loss of microfiber banding and less dense sheeting in the subfossil coral suggests

458 intensive structural degradation in the outermost, most seawater impacted region (Fig. 1C, 1D),
459 likely due to a combination of degradation with time and seawater exposure/infiltration. We
460 hypothesize that these physical changes could provide more surface area for microbial activity in
461 outer layers (Ingalls et al. 2003), in contrast to the denser, better protected inner layers. Finally,
462 we note that the physical transition from the outer layers' distinctive plate-like structure to more
463 dense layers in the inner layers appears gradual, and we could not clearly identify the distinct
464 chemical diagenetic horizon in SEM images which appeared quite sharp in the geochemical
465 proxies.

466 **4.2 Elemental Composition Changes**

467 The C/N ratio of unaltered gorgonin can be used as a reference to evaluate changes in
468 skeletal composition associated with degradation, since it should be both fixed and predictable
469 within any coral species. A similar C/N ratio approach has commonly been taken to assess both
470 diagenesis and exogenous organic contamination impacting the integrity of collagen, which has
471 structural similarities to gorgonin (e.g., Ambrose and Norr, 1992).

472 The C/N ratio of proteinaceous skeleton material from live-collected *K. haumeaae* in this
473 study (2.8 ± 0.1) agrees with a number of previous studies on live-collected *K. haumeaae* from
474 the Hawaii Islands (2.7-3.0 Sherwood et al., 2014, McMahon et al., 2015) and the Atlantic (2.8-
475 3.0 Druffel et al., 1995, Goodfriend 1997). It should be noted that most previous studies used
476 acidification prior to EA analysis to ensure no influence of inorganic carbonates on C/N ratios.
477 Prior published data using acidified samples (e.g., Guilderson et al., 2013, Glynn et al., 2019) has
478 shown indistinguishable C/N values from those we observed in our live-collected non-acidified
479 specimens, all suggesting that a C/N ratio of 2.7-3.0 would be expected for intact / non-degraded
480 *K. haumeaae* skeletons, which is similar to the expected C/N of pure protein (~3), and that

481 acidification does not change greatly these values for the intact organic matrix after any
482 carbonate is removed.

483 However, in our non-acidified subfossil skeleton samples, we observed elevated C/N
484 values (+0.1-0.8 C/N units higher versus the live-collected *K. haumeaae* skeleton; *results 3.2*;
485 Fig. 2). These findings corroborate a recent study showing that *non*-acidified subfossil coral C/N
486 values can deviate well above 3.0, particularly in outer exposed layers (Glynn et al. 2019). These
487 deviations suggest either carbonate precipitation or selective organic N loss with degradation in
488 exposed specimens. We also observed an essentially linear shift in C/N ratios in the subfossil
489 coral outer diagenetic horizon (0-10 mm), culminating in the highest C/N ratios at the seawater
490 interface (C/N = 3.7, Fig. 2A). Further, while acidification did reduce C/N ratios across the entire
491 coral transect, acidification did not "restore" C/N values in the outer diagenetic horizon to the
492 reference value. This strongly suggests that both carbonate formation and organic degradation
493 are simultaneously occurring. Finally, the fact that the inner skeleton layers of the subfossil coral
494 had C/N ratios within instrumental error to fresh gorgonin, regardless of acidification (average
495 offset +0.1 C/N units in >10 mm layers, research data 4), strongly indicates that inner skeleton
496 layers remain well protected from degradation even in a ~10 kyr specimen. Overall, we propose
497 C/N ratios *after* acidification can be used a simple metric to assess degradation state in non-
498 living coral sea floor specimens: C/N ratios >3 indicate appreciable degradation of the gorgonin
499 organic matrix, suggesting great caution in interpreting bulk $\delta^{13}C$ and $\delta^{15}N$ values (as discussed
500 in Sections 4.3-4.4). We recommend that future subfossil coral studies analyze C/N to test
501 degradation state prior to interpretation of environmental signatures.

502 **4.3 Mechanisms of elemental C/N and bulk $\delta^{13}C$ changes**

503 *4.3.1. Glycine loss*

504 The acidification tests described in Section 4.2 suggest that elevated C/N values are at
505 least in part due to the presence of secondary authigenic carbonate. However, a change in
506 organic gorgonin molecular composition is an additional possibility. While molecular AA data
507 indicate a relatively similar composition for most AAs between subfossil and live-collected coral
508 skeleton (Fig. 3B, results 3.3), glycine (Gly) was the major exception. The ~50% lower Gly
509 contribution in all layers of the subfossil specimen compared with modern gorgonin suggests a
510 major organic structural change. At the same time, Gly also has the lowest C/N value of any AA
511 (2.0). Therefore, the large loss of glycine must contribute at least in part to higher C/N values
512 observed throughout the subfossil skeleton. A mass balance calculation based on the modern
513 coral mol% values can broadly constrain this effect: our observed change in Gly from 52% in
514 live-collected skeleton to 23% in subfossil skeleton would be expected to increase C/N by 0.35-
515 0.41, assuming that all other organic composition remains constant. We note that while
516 acidification results show this cannot be the only process at work, at the same time this result is
517 quite similar to the actual C/N offsets observed between the subfossil inner layers (>10 mm) and
518 the average of modern corals (research data 3). One caveat to this estimate is that our acid
519 hydrolysis-based analytical method cannot measure Histidine. Histidine is an N-rich (low C/N)
520 AA that is very abundant in many gorgonin-based proteins (18-30%; Druffel et al., 1995,
521 Goodfriend, 1997) such that any major "hidden" changes in this AA could have substantial C/N
522 impacts. However, the fact that our simple calculation based on Gly loss alone is consistent with
523 both observed C/N and molar data suggests that loss of glycine is likely the dominant organic
524 process driving the C/N offset between modern and subfossil corals over millennial timescales.
525 The mechanism leading to large glycine losses from coral skeleton over millennia is
526 uncertain. However, the fact Gly appears to be lost and not gained in subfossil corals compared

527 with modern corals, coupled with only minor changes in other AA molar composition (results
528 3.3), strongly suggests an abiotic mechanism. Gly mol% increases are a widely used AA
529 indicator for microbial degradation (e.g., Dauwe et al., 1999; Yamashita and Tanoue, 2003;
530 Kaiser and Benner, 2009), making a nearly 50% Gly reduction inconsistent with typical
531 biologically-mediated changes. Further the widely used Degradation Index (DI; based on AA
532 mol% shifts observed with marine organic matter degradation; Dauwe et al., 1999) yields DI
533 values close to "fresh" plankton in the inner coral (Fig. S8). In fact, most of the subfossil coral
534 DI values *elevated* (indicating *less* degradation) versus the values of the modern coral specimen.
535 As discussed further below (section 4.5) this is likely due in part to the unique AA composition
536 of the gorgonin skeleton, rather than microbial degradation of subfossil coral skeleton.
537 We hypothesize that abiotic glycine decarboxylation may be the main mechanism for
538 subfossil coral Gly loss. The spontaneous aqueous decarboxylation of free glycine is well
539 known, whereby water molecules assist with proton transfer cleaving the Gly C-N bond,
540 resulting in degradation of Gly (e.g., Catão and López-Castillo, 2018 and references within). As
541 structurally the simplest of all AAs, glycine ($C_2H_5NO_2$) is thermodynamically favored to remove
542 the amide group to form bicarbonate and also requires the least water ($4H_2O$) to do so (LaRowe
543 and Van Cappellen, 2011). We note that this process may also contribute to authigenic carbonate
544 formation, potentially accounting for some of the C/N offset between the acidified and non-
545 acidified data. While this reaction has not been previously reported for glycine bound in a
546 proteinaceous structure, it would provide a potential mechanism for Gly degradation in the
547 seawater exposed outer diagenetic horizon of coral skeletons over ~10 kyrs.
548 Gly loss would also be consistent with physical structure changes, as Gly plays an
549 important role in holding adjacent layers together in *K. haumeaae* skeletons (Druffel et al. 1995).

550 We therefore further hypothesize that selective abiotic Gly loss contributes to the altered
551 physical matrix observed in subfossil coral SEM images (Fig. 1A, B). Finally, we note that while
552 the dramatic Gly molar depletion (~50%) is clear in all subfossil coral samples, the more minor
553 Gly changes observed from inner vs. outer subfossil skeleton (~5 mol%; Fig. 3) are in the
554 opposite direction. While these more minor offsets are approaching the analytical variation of
555 chromatography methods, this result at least suggests that some addition biotic degradation of the
556 protein matrix is occurring, superimposed on the earlier rapid and far larger abiotic
557 decarboxylation. Investigation into whether AA degradation in protein-bound AAs follows the
558 same hydrolysis-based degradation pathways as free AAs is necessary to validate this
559 hypothesis. Such work would shed additional light on other unknown compounds besides the
560 dominant proteinaceous material in these types of deep-sea corals that may also be altered during
561 this degradation process.
562
563 *4.3.2 Secondary authigenic carbonate*
564 Higher C/N ratios and $\delta^{13}C$ values observed after acidification must in part be due to
565 carbonate precipitation, particularly in the outermost coral layers (0-10 mm) most subjected to
566 seawater infiltration. Though of note, even if the inner layers (>10 mm) are protected from direct
567 seawater influence, if our hypothesis regarding Gly decarboxylation is correct then inorganic
568 carbonate could also accumulate here (Catão and López-Castillo, 2018). While seawater
569 carbonate precipitation is therefore never mutually exclusive from an abiotic decarboxylation
570 mechanism, one major difference is that carbonate precipitation should lead to a
571 contemporaneous increase in bulk $\delta^{13}C$ values. Glycine loss is more difficult to constrain,
572 however it would most likely work in the opposite direction (i.e., *decreasing* bulk $\delta^{13}C$ values),

573 because Gly is typically ~3‰ higher in $\delta^{13}C$ value compared to the average of all proteinaceous
574 AAs (Shen et al. 2021, McCarthy et al., 2013).

575 As carbonate $\delta^{13}C$ endmembers can be estimated, the potential quantitative influence of
576 authigenic carbonate on bulk $\delta^{13}C$ values can be constrained using isotope mass balance. If we
577 assume a $\delta^{13}C$ value of 1‰ for dissolved inorganic carbon (DIC) and a fractionation (ε) from
578 DIC to calcite of 1‰, then authigenic calcite should have a $\delta^{13}C$ value of ~2‰ (Romanek et al.,
579 1992; Quay et al., 2003). This means that the maximum observed offset of ~1.4‰ between the
580 acidified and non-acidified samples in the outermost 1 mm (Fig. 2C) would require ~7-8% of
581 total C to be present as calcite precipitate. Returning to our C/N data, if the "fresh" gorgonin C/N
582 is ~2.8, then 8% carbonate accumulation (as a fraction of total C) would cause C/N to increase to
583 ~3.0. This shift of ~0.2 C/N would therefore represent approximately half of the ~0.4 C/N shift
584 we calculated above from loss of glycine.

585 Currently no studies have focused on carbonate precipitation in deep-sea proteinaceous
586 coral skeletons. Estimates of sedimentary secondary authigenic carbonate formation can reach as
587 high as 10% in high depositional regions (Sun and Turchyn, 2014). While the mechanism for
588 sedimentary authigenic carbonate formation is clearly different than in deep-sea corals, and in
589 particular is likely much more dependent on pH and degrading organic matter, nevertheless we
590 note that the similar magnitudes of maximum carbonate in our outer coral layers and in
591 sediments at least suggest that this mass balance estimate of possible secondary authigenic
592 carbonate formation is not unreasonable. Some additional carbonate precipitation could also be
593 related to respiration of the skeletal organic matter should seawater intrusion supply enough
594 oxygen that pH does not facilitate dissolution. Particularly in the outer diagenetic horizon, both
595 processes are likely contributing to observed isotope shifts. For sediments, locations with

enhanced microbial respiration tend to have the largest amount of authigenic carbonate formation, because microbes affect pore water chemistry by converting organic matter to CO_2, which then precipitates as carbonate (e.g., Sun and Turchyn, 2014). Further analysis to discover whether unique microbial populations facilitate deep-sea coral degradation and how the deposition and degradation of sediments upon dead skeletons impact water chemistry should be conducted.

4.4 Biological degradation in seawater exposed gorgonin: impact on bulk $\delta^{15}N$ values and CSIA-AA parameters

In contrast to the protected inner layers, the outer diagenetic horizon (0-10 mm) layers show clear evidence of microbial degradation, discernible at the molecular level. While carbonate precipitation and abiotic Gly loss described in Section 4.3.1 can account for some of the C/N and isotope ratios changes (Fig. 2), the $\delta^{15}N_{AA}$ values in the outer layers bear the signature of microbial resynthesis with highly elevated ΣV values in comparison to both the modern coral specimen and the subfossil coral interior (McCarthy et al., 2007: Fig. 6C). The ΣV parameter quantifies variability in $\delta^{15}N_{AA}$ patterns as a measure of progressive degradation and reflects the selective microbial resynthesis of individual AAs (McCarthy et al., 2007, Batista et al., 2014, Sauthoff et al., 2016, Ohkouchi et al, 2017). Together with strongly elevated bulk $\delta^{15}N$ values, ecologically unrealistic CSIA-AA trophic position values (Fig. 6D; discussed in Section 4.4.1), and dramatic outer layer structural changes seen in SEM imaging (Fig. 1), this data suggest significant biological degradation of the outer gorgonin matrix after direct contact with seawater.

We propose that the coupled large changes in bulk $\delta^{15}N$ and $\delta^{13}C$ values observed in the diagenetic horizon likely reflect combined abiotic and biological effects of oxic seawater

619 exposure. Multiple lines of evidence support this conclusion. First, the large and almost linear
620 increase in $\delta^{15}N$ values of ~7‰ in the outer layers is consistent with expected impact of
621 microbial degradation on organic matter, typically imparting a strong increase in the $\delta^{15}N$ values
622 of the residual or substrate organic matter, with changes in $\delta^{15}N$ values up to 6‰ observed in
623 sediments and suspended particles (Saino and Hattori, 1980; Saino and Hattori, 1987; Altabet,
624 1988; Lehmann et al., 2002). While some baseline $\delta^{15}N$ shift cannot be ruled out, the
625 unidirectional change in $\delta^{15}N$ values in the outer coral is substantially greater than any
626 documented change in comparable corals since at least the last 5 kyrs (Williams and Grottoli,
627 2010, Sherwood et al., 2014, Glynn et al. 2019). This suggests $\delta^{15}N$ baseline changes are
628 exceedingly unlikely to be the main driver of the $\delta^{15}N$ change in the outer diagenetic horizon.
629 Second, some part of the $\delta^{13}C$ value increases may also be due to microbial degradation
630 removing the lighter ^{12}C from the skeleton, in addition to respiration contributing to carbonate
631 formation discussed in Section 4.3.2. Given that our isotope mass balance exercise above
632 suggests ~1‰ of the observed $\delta^{13}C$ change could be due to carbonate formation, this would
633 theoretically leave another ~1‰ of the total shift observed in the outer layers due to a
634 mechanism like microbial degradation.

635 Finally, we also evaluated the degradation index (DI) because is one of the most widely
636 used degradation proxies in organic geochemistry, commonly applied in sediments, ocean
637 particles, and other detrital organics (Dauwe et al., 1999). The underlying assumption of the DI
638 index is that AAs have different and predictable relative lability to bacterial degradation of
639 proteinaceous materials. However, the standard DI formulation does not appear to indicate
640 lability in gorgonin as DI indicated more “degraded” values in the most protected inner coral
641 layers, becoming “fresher” with progressive structural deterioration and alteration of other

642 degradation metrics (Fig. S8). In particular in the outer diagenetic horizon where evidence of
643 degradation seems unambiguous, DI does not change in a uniform manner. We hypothesize that
644 either the very different AA composition of gorgonin (a very specific, single structural protein),
645 or different mechanisms by which bacteria are able to degrade this material, underlie these
646 observations. We conclude that standard DI is not a useful metric to evaluate relative degradation
647 state/integrity of gorgonin structural protein but by utilizing skeletons spanning a variety of ages
648 it should be possible to create a coral specific DI.

649 *4.4.1 Preservation and likely fidelity of CSIA-AA parameters*

650 Degradation in the outer diagenetic horizon had major impacts on two important CSIA-
651 AA proxies of environmental biogeochemistry and trophic dynamics. $TP_{CSIA\text{-}AA}$ is commonly
652 applied in deep sea corals and sediments to indicate relative changes in planktonic food web
653 structure (Batista et al. 2014, Sherwood et al. 2014, Sauthoff et al., 2016). It appears that
654 microbial degradation in the outer subfossil coral material also strongly impacts $TP_{CSIA\text{-}AA\ Skeleton}$,
655 consistent with elevated ΣV data in this zone. Specifically, the lowest $TP_{CSIA\text{-}AA\ Skeleton}$ value of
656 1.7 in the outer subfossil coral layers is more than a full trophic step lower than the inner (>10
657 mm) layers ($TP_{CSIA\text{-}AA\ Skeleton}$ = 3.1 ± 0.1), with swings of ~1.5 trophic levels between adjacent
658 samples (Fig. 6D). It seems very unlikely that large and rapid shifts in overlying plankton
659 ecology and unrealistically low TP values occur only at the end of this coral colony's millennial
660 lifespan. We note that the mean trophic–source $\delta^{15}N_{AA}$ offsets, often used as proxy for relative
661 TP change that avoids issues of TDF and β selection, (McCarthy et al. 2007, Sherwood et al.
662 2011, Batista et al. 2014), show similar patterns. Together, these data indicate that TP_{CSIA} values
663 are viable in the intermediate (transition) and inner most protected coral regions, but should not

664 be trusted in the outer diagenetic horizon without corroborating evidence of minimal degradation
665 (i.e., ΣV value and/or C/N ratio).

666 The significantly higher ΣV values in the outer zone of the subfossil coral skeleton
667 (maximum 5.8, Fig. 6C) were clearly distinct from both the inner zone and modern corals and
668 were consistent with strong microbial resynthesis. The ΣV values (3-4) observed throughout the
669 inner subfossil coral are high relative to the range typically found in plankton or non-degraded
670 proteinaceous materials (<2.0; McCarthy et al, 2007), and slightly elevated compared to modern
671 coral specimens (~3.0; Sherwood et al., 2014; this study, Fig. 6). In the modern coral, the
672 difference in ΣV value from fresh material has been attributed to the unique AA composition of
673 the gorgonin structural protein (Sherwood et al., 2014). However, note that the ~1 ΣV value
674 offset between modern and inner subfossil coral layers is almost exclusively driven by changes
675 in isoleucine. Without isoleucine, both modern and subfossil ΣV values are very similar (0.4 ΣV
676 offset), which is consistent with the very similar CSIA-AA biosynthetic patterns (Fig. 5, 6B).
677 This apparently singular $\delta^{15}N$ shift in isoleucine in the subfossil coral is puzzling. A unique
678 isoleucine shift of this kind has never been observed in CSIA-AA $\delta^{15}N$ patterns for degrading
679 OM; in fact here it might not be biological at all, given that it is observed even in the innermost,
680 protected coral layers. Further research into this loss could shed more light on the mechanisms
681 underlying multi-millennial gorgonin alteration. Overall, bulk $\delta^{15}N$ values and $\delta^{15}N_{AA}$ patterns
682 for all other AAs indicates that CSIA-AA proxies were well preserved in the inner coral layers
683 with the only exception being the trophic AA Ile. Similarly, with the exception of Ile and the
684 metabolic AA Thr, the scatter of the individual non-normalized as well as THAA-normalized
685 values in the ≥10 mm interior of the sub-fossil specimen were similar to the scatter in not only

686 the modern Cross Seamount specimen, but a larger data-set in near-modern specimens from off
687 Oahu (Sherwood et al., 2014) (Fig. S3-S6).
688
689 **4.5 Inner coral preservation of CSIA-AA parameter integrity**
690 The excellent preservation of expected molecular geochemistry parameters (e.g., mol%,
691 ΣV, TP_{CSIA}) in the inner coral (>10 mm) strongly suggests that beyond the outer diagenetic
692 horizon, subfossil deep-sea proteinaceous skeletons remain viable as paleoenvironmental
693 bioarchives. As baseline $\delta^{13}C$ or $\delta^{15}N$ values of primary production from ~9.6-11.6 kyr BP
694 cannot be known, it is not possible to directly confirm this hypothesis. However, there are ways
695 to evaluate the integrity of CSIA-AA values by examining CSIA-AA patterns and source AA
696 values in order to reconstruct paleo-export production values.
697 The first way is specifically evaluating relative CSIA-AA *patterns* with those from
698 marine primary production and sinking particles (Fig. S9). The observation of expected *patterns*
699 in normalized CSIA-AA data provides strong evidence for the preservation of individual AA
700 isotope *values* since degradation processes scrambles CSIA-AA patterns and degradation is
701 unlikely to alter values of every AA in exactly the same way (e.g. McCarthy et al., 2007,
702 Okhouchi et al., 2017). The essentially identical $\delta^{15}N_{norm\text{-}AA}$ patterns observed for almost all AAs
703 (Fig. 5; Results 3.5) in the inner (>10 mm) zone of the subfossil coral match those CSIA-AA
704 biosynthetic patterns expected for live-collected deep sea corals, which consume photosynthetic
705 marine algae and sinking particles (Fig. S9; Shen et al., 2021, McCarthy et al., 2013, this study).
706 Average source and trophic AA group values can represent an additional check on the influence
707 of any possibly anomalous individual AA isotope changes with degradation (McCarthy et al.,
708 2007). Both these metrics also show stable plateaus for the inner (>10 mm) layers of the

subfossil coral (Fig. 6), consistent with the relatively low and stable ΣV values described earlier, and again supporting good preservation of CSIA-AA $\delta^{15}N$ values in the protected interior coral skeleton.

A second way to evaluate if AA values have been well preserved is to ask if shifts in predicted 'baseline" correspond with records from other archives in this region. The shift in "baseline" $\delta^{15}N$ values indicated by CSIA-AA (e.g., Source AA's Lys, Phe, Tyr; non-normalized) are in fact consistent with expected changes in this Pacific region. The shift in average source AA values indicates a change in the source nitrate $\delta^{15}N$ value of ~3‰ between the subfossil inner layers (10-11.6 kyrs BP; $\delta^{15}N_{source}$= 9.4 ± 0.5‰) and the modern coral ($\delta^{15}N_{source}$= 6.3 ± 1.3‰, research data 8 and 9). Based on the molecular changes found in this study, such as the shift in Gly from 52-26%, these composition changes may account for a ~1‰ increase in bulk $\delta^{15}N$ over this timeframe. This would account for a third of the ~3‰ change between modern and inner subfossil, leaving ~2‰ attributed to environmental change, which is still within range suggested by sedimentary margin records (~1-5‰; Tesdal et al. 2013). The CSIA-AA $\delta^{13}C$ (mol% weighted THAA; a proxy for baseline) also supports a baseline shift between the modern coral (-9.9 ± 0.7‰; n = 3) and the subfossil coral (-11.9 ± 0.2‰; n = 6), again consistent with the export production $\delta^{13}C$ values that have increased by ~2‰ from the Younger Dryas (~12 kyrs ago) to the late Holocene in Pacific Margin sedimentary $\delta^{13}C$ records (references within Tesdal et al. 2013). Together these results also suggest that $\delta^{13}C_{AA}$ plankton community fingerprinting approaches recently demonstrated in ~1000 yr old gold corals (McMahon et al., 2015) may also be able to reconstruct plankton community structure of exported production from subfossil corals, assuming that proper phytoplankton end-members are used for a given time period.

5. Summary and Conclusions

By comparing a subfossil (~9.6-11.6 kyr BP) *K. haumeaae* coral skeleton with a live-collected specimen from the same seamount in Hawaii, this study documented microstructural, molecular, and geochemical changes accompanying degradation of the proteinaceous coral gorgonin matrix. These changes occurred primarily in the outermost skeleton, which we hypothesize are due to a combination of abiotic and biotic degradation as a function of contact with oxic seawater for ~10 kyr. The physical structure of the outer subfossil coral showed pronounced loss of banding, shifting to a randomized plate-like and presumably less dense structure. We hypothesize that these structural changes contributed to seawater penetration and subsequent microbial activity that altered skeleton molecular and geochemical values in this outer diagenetic horizon. At the molecular level, all layers of the subfossil coral had only about half the expected molar glycine content of live-collected coral skeleton, while the effects of acidification on skeleton $\delta^{13}C$ values indicated significant authigenic carbonate formation, particularly in the outer zone. We hypothesize that this carbonate formation was enhanced by the abiotic degradation of glycine and associated production of bicarbonate. However, despite all these changes, molar compositions for all other AAs were similar to the live-collected counterpart for all but the outermost (0-10 mm) layers.

The outermost ~10 mm of the subfossil coral was distinct in every molecular parameter, with extensive changes consistent with both microbial degradation and substantial carbonate precipitation, both likely linked to seawater exposure. Large linear increases in bulk $\delta^{13}C$ and $\delta^{15}N$ values, coupled with high values of the degradation parameter ΣV and anomalous CSIA-AA trophic position values indicated extensive, progressive, and easily identifiable microbial degradation. Together, these shifts are consistent with progressive organic degradation with

755 seawater infiltration and attendant gorgonin physical structure breakdown, occurring in this coral
756 at approximately 1 mm per 1000 yrs.

757 In contrast to the outer diagenetic horizon, all the same proxies within the intermediate
758 and innermost coral layers indicated excellent preservation of the gorgonin protein, in particular
759 molecular level AA isotope values. We propose C/N ratio as a basic metric to evaluate skeleton
760 integrity, where C/N values above 3 for this species indicate degradation extensive enough to
761 confound bulk isotope data interpretations. This should be supplemented by acid tests (or direct
762 %$CaCO_3$ determination) to evaluate carbonate contamination. Further, we suggest that while the
763 DI index appears to not function reliably in the gorgonin matrix, the CSIA-AA based ΣV metric
764 beyond the typical gorgonin baseline value of 3.0 can provide clear information about microbial
765 influence.

766 While gorgonin bulk isotope and elemental values can be strongly altered in the outer
767 zone of subfossil specimens, CSIA-AA values and associated proxies appear to be far more
768 robust to these degradation processes. In particular CSIA-AA proxies for isotopic baseline (Phe,
769 mean source AA $\delta^{15}N$ values, and mean essential AA $\delta^{13}C$ values) appeared to be well preserved
770 beyond the outer diagenetic horizon, with biosynthetic patterns very similar to both primary
771 production and modern coral gorgonin for both $\delta^{13}C$ and $\delta^{15}N$ values. Even Gly, despite its very
772 large molar loss, had normalized CSIA-AA patterns that matched those expected from modern
773 corals for both $\delta^{13}C$ and $\delta^{15}N$. The $\delta^{15}N$ values of Ile were one notable exception, with
774 substantially elevated $\delta^{15}N$ values in all zones of the subfossil coral. To our knowledge, such
775 shifts in Ile $\delta^{15}N$ values have not been previously observed, and based on these observations, we
776 suggest that ΣV in protein corals should in the future be calculated without Ile.

Overall, the excellent CSIA-AA pattern preservation in the inner deep-sea proteinaceous coral skeletons on multi-millennial time scales indicates that source and essential AAs can be used to determine environmental information about export production and degradative processes in subfossil coral skeletons when C/N and ΣV values fall within expected ranges. We propose that a combination of elemental and CSIA-AA metrics can be used to readily gauge gorgonin integrity and screen subfossil samples for more reliable geochemical interpretations. This work opens wide potential to the use of CSIA-AA proxies for reconstructing baseline biogeochemical cycling, export production dynamics, and algal trophic structure and community composition, at least back through the Holocene using the wealth of available subfossil specimens.

Acknowledgements

None of this work would have been possible without the captain and crew of the RV Ka‘imikai-o-Kanaloa and the pilots and engineers of the Hawai’i Undersea Research Lab. Sample collection was funded by NOAA/NURP and the National Geographic Society (7717-04). A portion of this work was performed under the auspices of the U.S. Department of Energy (DE-AC52-07NA27344). The majority of the work presented here was funded by the National Science Foundation (OCE 1061689). D.S. Glynn was supported by a Eugene Cota-Robles Fellowship and a National Science Foundation Graduate Research Fellowship (NSF-GRFP; 1339067). We acknowledge Dr. T. Yuzvinsky for assistance with sample preparation and electron microscopy and the W.M. Keck Center for Nanoscale Optofluidics for use of the FEI Quanta 3D Dualbeam microscope. Further thanks go to D. Andreasen, C. Carney, R. Franks and a team of undergrad interns (S. Kaplan, A. Jalali-Sohi, K. Miles, L. Gomez, Z. Wright) for laboratory assistance. Thanks to the assisting editors and anonymous reviewers for their feedback.

References

Altabet M. A. (1988) Variations in nitrogen isotopic composition between sinking and suspended particles: implications for nitrogen cycling and particle transformation in the open ocean. *Deep Sea Research Part A. Oceanographic Research Papers* **35**, 535–554.

Ambrose S.H. and Norr L. (1993) Experimental Evidence for the Relationship of the Carbon Isotope Ratios of Whole Diet and Dietary Protein to Those of Bone Collagen and Carbonate. In *Prehistoric Human Bone* (eds. J. B. Lambert, G. Grupe). Springer. pp. 1–38.

821 Batista F. C., Ravelo C. A., Crusius J., Casso M. A., and McCarthy M. D. (2014) Compound
822 specific amino acid $\delta^{15}N$ in marine sediments: A new approach for studies of the marine
823 nitrogen cycle. *Geochimica et Cosmochimica Acta* **142**, 553–569.
824 Boyer T. P., Garcia H. E., Locarnini R. A.; Zweng M. M., Mishonov A. V., Reagan J. R.,
825 Weathers K. A., BaranovaO. K., Seidov D., Smolyar I. V. (2018) World Ocean Atlas
826 2018. Temperature and Dissolved Oxygen averaged over years 1955-2010 at 400m.
827 *NOAA National Centers for Environmental Information,*
828 https://accession.nodc.noaa.gov/NCEI-WOA18 (accessed July-4-2021).
829 Chikaraishi Y., Ogawa N.O., Kashiyama Y., Takano Y., Suga H., Tomitani A., Miyashita H.,
830 Kitazato H., and Ohkouchi N. (2009) Determination of aquatic food-web structure based
831 on compound-specific nitrogen isotopic composition of amino acids. *Limnology and*
832 *Oceanography: Methods* **7**, 740–750.
833 Dauwe B., Middelburg J. J., Herman P. M. J., and Heip C.H.R. (1999) Linking diagenetic
834 alteration of amino acids and bulk organic matter reactivity. *Limnology and*
835 *Oceanography* **44**, 1809–1814.
836 Druffel E. R. M., Griffin S., Witter A., Nelson E., Southon J., Kashgarian M., and Vogel J.
837 (1995) Gerardia: Bristlecone pine of the deep-sea? *Geochimica et Cosmochimica Acta*
838 **59**, 5031–5036.
839 Edinger E. N. and Sherwood O. A. (2012). Applied taphonomy of gorgonian and antipatharian
840 corals in Atlantic Canada: experimental decay rates, field observations, and implications
841 for assessing fisheries damage to deep-sea coral habitats. *Neues Jahrbuch fur Geologie*
842 *und Palaontologie-Abhandlungen*, **265**, 199.

843 Ehrlich H. (2010) Chitin and collagen as universal and alternative templates in biomineralization.
844 *International Geology Review* **52**, 661-699.
845 Glynn D. S., McMahon K. W., Guilderson T. P., and McCarthy M. D. (2019) Major shifts in
846 nutrient and phytoplankton dynamics in the North Pacific Subtropical Gyre over the last
847 5000 years revealed by high-resolution proteinaceous deep-sea coral $\delta^{15}N$ and $\delta^{13}C$
848 records. *Earth and Planetary Science Letters* **515**, 145–153.
849 Goldberg W. M. (1974) Evidence of a sclerotized collagen from the skeleton of a gorgonian
850 coral. *Comparative Biochemistry and Physiology Part B: Comparative Biochemistry* **49**,
851 525–526.
852 Goldberg W. M. (1976) Comparative study of the chemistry and structure of gorgonian and
853 antipatharian coral skeletons. *Marine Biology* **35**, 253–267.
854 Goodfriend G. A. (1997) Aspartic acid racemization and amino acid composition of the organic
855 endoskeleton of the deep-water colonial anemone Gerardia : Determination of longevity
856 from kinetic experiments. *Geochimica et Cosmochimica Acta* **61**, 1931–1939.
857 Guilderson T. P., McCarthy M. D., Dunbar R. B., Englebrecht A., and Roark, E.B. (2013) Late
858 Holocene variations in Pacific surface circulation and biogeochemistry inferred from
859 proteinaceous deep-sea corals. *Biogeosciences* **10**, 6019–6028.
860 Guilderson T. P., Schrag D. P., Druffel E. R. M., Reimer R. W. (2021) Postbomb Subtropical
861 North Pacific Surface Water Radiocarbon History. *Journal of Geophysical Research:*
862 *Oceans* **126**, e2020JC016881.
863 Heaton T. J., Köhler P., Butzin M., Bard E., Reimer R. W., Austin W.E.N., Bronk Ramsey C.,
864 Grootes P.M., Hughen K. A., Kromer B., Reimer P. J., Adkins J., Burke A., Cook M. S.,

865 Olsen J., Skinner L. C. (2020) Marine20 - The Marine Radiocarbon Age Calibration
866 Curve (0-55,000 cal BP). *Radiocarbon* **62**, 779–820.
867 Hendy J. (2021) Ancient protein analysis in archaeology. *Science Advances*,
868 10.1126/sciadv.abb9314.
869 Hill T. M., Myrvold C. R., Spero H. J., and Guilderson T. P. (2014) Evidence for benthic-pelagic
870 food web coupling and carbon export from California margin bamboo coral archives.
871 *Biogeosciences* **11**, 3845–3854.
872 Holl S. M., Schaefer J., Goldberg W. M., Kramer K. J., Morgan T. D., and Hopkins T. L. (1992)
873 Comparison of Black Coral Skeleton and Insect Cuticle by combination of Carbon-13
874 NMR and Chemical Analyses. *Archives of Biochemistry and Biophysics,* **292,** 107-111.
875 Ingalls A. E., Lee C., and Druffel E. R. M. (2003) Preservation of organic matter in mound-
876 forming coral skeletons. *Geochimica et Cosmochimica Acta* **67**, 2827–2841.
877 Kaiser K. and Benner R. (2009) Biochemical composition and size distribution of organic matter
878 at the Pacific and Atlantic time-series stations. *Marine Chemistry* **113**, 63-77.
879 Krull E. S., Baldock J. A., and Skjemstad J.O. (2003) Importance of mechanisms and processes
880 of the stabilization of soil organic matter for modelling carbon turnover. *Functional Plant*
881 *Biology* **30**, 207–222.
882 LaRowe D. E. and Van Cappellen P. (2011) Degradation of natural organic matter: A
883 thermodynamic analysis. *Geochimica et Cosmochimica Acta* **75**, 2030-2042.
884 Larsen T., Ventura M., Andersen N., O'Brien D. M., Piatkowski U., and McCarthy, M. D.
885 (2013). Tracing carbon sources through aquatic and terrestrial food webs using amino
886 acid stable isotope fingerprinting. *PloS one* **8**, e73441.

887 Le Campion Alsumard T., Golubic S., and Hutchings P. (1995) Microbial endoliths in skeletons
888 of live and dead corals: Porites lobata (Moorea, French Polynesia). *Marine Ecology*
889 *Progress Series* **117**, 149–158.
890 Lehmann M. F., Bernasconi S. M., Barbieri A., and McKenzie J. A. (2002) Preservation of
891 organic matter and alteration of its carbon and nitrogen isotope composition during
892 simulated and in situ early sedimentary diagenesis. *Geochimica et Cosmochimica Acta*
893 **66**, 3573–3584.
894 Catão A. J. L. and López-Castillo A. (2018) On the degradation pathway of glyphosate and
895 glycine. *Environmental Science: Processes and Impacts* **20**, 1148-1157.
896 McCarthy M. D., Benner R., Lee C. and Fogel M. L. (2007) Amino acid nitrogen isotopic
897 fractionation patterns as indicators of heterotrophy in plankton, particulate, and dissolved
898 organic matter. *Geochimica et Cosmochimica Acta* **71**, 4727–4744.
899 McCarthy M. D., Lehman J., and Kudela R. (2013) Compound-specific amino acid $\delta^{15}N$ patterns
900 in marine algae: Tracer potential for cyanobacterial vs. eukaryotic organic nitrogen
901 sources in the ocean. *Geochimica et Cosmochimica Acta* **103**, 104-120.
902 McMahon K. W., Fogel M. L., Elsdon T. S., and Thorrold, S. R. (2010). Carbon isotope
903 fractionation of amino acids in fish muscle reflects biosynthesis and isotopic routing from
904 dietary protein. *Journal of Animal Ecology* **79**, 1132-1141.
905 McMahon K. W., McCarthy M. D., Sherwood O. A., Larsen T., and Guilderson T. P. (2015)
906 Millennial-scale plankton regime shifts in the subtropical North Pacific Ocean. *Science*
907 **350**, 1530–1533.

McMahon K. W. and McCarthy M. D. (2016) Embracing variability in amino acid $\delta^{15}N$ fractionation: Mechanisms, implications, and applications for trophic ecology. *Ecosphere* **7**, 1–26.

McMahon K. W., Williams B., Guilderson T. P., Glynn D. S., and McCarthy M. D. (2018) Calibrating amino acid $\delta^{13}C$ and $\delta^{15}N$ offsets between polyp and protein skeleton to develop proteinaceous deep-sea corals as paleoceanographic archives. *Geochimica et Cosmochimica Acta* **220**, 261-275.

Nielsen J. M., Popp B. N., and Winder M. (2015). Meta-analysis of amino acid stable nitrogen isotope ratios for estimating trophic position in marine organisms. *Oecologia* **178**, 631-642.

Noé S. U. and Dullo W. C. (2006). Skeletal morphogenesis and growth mode of modern and fossil deep-water isidid gorgonians (Octocorallia) in the West Pacific (New Zealand and Sea of Okhotsk). *Coral reefs,* **25**, 303-320.

Noé S., Lembke-Jene L., Reveillaud J., and Freiwald A. (2007). Microstructure, growth banding and age determination of a primnoid gorgonian skeleton (Octocorallia) from the late Younger Dryas to earliest Holocene of the Bay of Biscay. *Facies*, **53**, 177-188.

Ohkouchi N., Chikaraishi Y., Close H. G., Fry B., Larsen T., Madigan D. J., McCarthy M. D., McMahon K. W., Nagata T., Naito Y. I., Ogawa N. O., Popp B. N., Steffan S., Takano Y., Tayasu I., Wyatt A. S. J., Yamaguchi Y. T., and Yokoyama Y. (2017) Advances in the application of amino acid nitrogen isotopic analysis in ecological and biogeochemical studies. *Organic Geochemistry* **113**, 150-174.

929 Quay P., Sonnerup R., Westby T., Stutsman J., McNichol A. (2003) Changes in the $^{13}C/^{12}C$ of
930 dissolved inorganic carbon in the ocean as a tracer of anthropogenic CO_2 uptake. *Global*
931 *Biogeochemical Cycles* **17**, 1004.
932 Ramirez M. D., Besser A. C., Newsome S. D., and McMahon K. W. (2021) Meta-analysis of
933 primary producer amino acid δ15N values and the ir influence on trophic position
934 estimation. *Methods Ecol Evol.* **12**, 1750–1767.
935 Roark E. B., Guilderson T. P., Dunbar R. B., and Ingram B. L. (2006) Radiocarbon-based ages
936 and growth rates of Hawaiian deep-sea corals. *Marine Ecology Progress Series* **327**, 1–
937 14.
938 Romanek C. S., Grossman E. L., and Morse J.W. (1992) Carbon isotopic fractionation in
939 synthetic aragonite and calcite: Effects of temperature and precipitation rate. *Geochimica*
940 *et Cosmochimica Acta* **113**, 150–174.
941 Saino T. and Hattori A. (1980) ^{15}N natural abundance in oceanic suspended particulate matter.
942 *Nature* **283**, 752–754.
943 Saino T. and Hattori A. (1987) Geographical variation of the water column distribution of
944 suspended particulate organic nitrogen and its ^{15}N natural abundance in the Pacific and its
945 marginal seas. *Deep Sea Research Part A, Oceanographic Research Papers* **34**, 807–827.
946 Sauthoff W. (2016) Nitrogen Isotopes of Amino Acids in Marine Sediment: A Burgeoning Tool
947 to Assess Organic Matter Quality and Changes in Supplied Nitrate ^{15}N. University of
948 California Santa Cruz, Master's Thesis.
949 Schiff J. T., Batista F. C., Sherwood O. A., Guilderson T. P., Hill T. M., Ravelo A. C., McMahon
950 K. W. and McCarthy M. D. (2014) Compound specific amino acid $\delta^{13}C$ patterns in a

951 deep-sea proteinaceous coral: Implications for reconstructing detailed $\delta^{13}C$ records of
952 exported primary production. *Marine Chemistry* **166**, 82–91.
953 Shen Y., Guilderson T. P., Sherwood O. A., Castro C. G., Chavez F. P. and McCarthy M. D.
954 (2021) Amino acid $\delta^{13}C$ and $\delta^{15}N$ patterns from sediment trap time series and deep-sea
955 corals: Implications for biogeochemical and ecological reconstructions in paleoarchives.
956 *Geochimica et Cosmochimica Acta* **297**, 288–307.
957 Sherwood O. A., Guilderson T. P., Batista F. C., Schiff J. T. and McCarthy M.D. (2014)
958 Increasing subtropical North Pacific Ocean nitrogen fixation since the Little Ice Age.
959 *Nature* **505**, 78–81.
960 Sherwood O. A. and Edinger E. N. (2009) Ages and growth rates of some deep-sea gorgonian
961 and antipatharian corals of Newfoundland and Labrador. *Canadian Journal of Fisheries*
962 *and Aquatic Sciences* **66**, 142–152.
963 Sherwood O. A., Lehmann M. F., Schubert C. J., Scott D. B. and McCarthy M. D. (2011)
964 Nutrient regime shift in the western North Atlantic indicated by compound-specific $\delta^{15}N$
965 of deep-sea gorgonian corals. *Proceedings of the National Academy of Sciences of the*
966 *United States of America* **108**, 1011–1015.
967 Sherwood O. A., Scott D. B. and Risk M. J. (2006) Late Holocene radiocarbon and aspartic acid
968 racemization dating of deep-sea octocorals. *Geochimica et Cosmochimica Acta* **70**, 2806–
969 2814.
970 Sherwood O. A., Thresher R. E., Fallon S. J., Davies D. M. and Trull T.W. (2009) Multi-century
971 time-series of ^{15}N and ^{14}C in bamboo corals from deep Tasmanian seamounts: Evidence
972 for stable oceanographic conditions. *Marine Ecology Progress Series* **397**, 209–218.

973 Silfer J. A., Engel M. H., Macko S. A. and Jumeau E. J. (1991) Stable carbon isotope analysis of
974 amino acid enantiomers by conventional isotope ratio mass spectrometry and combined
975 gas chromatography/isotope ratio mass spectrometry. *Analytical Chemistry* **63**, 370–374.
976 Strzepek K. M., Thresher R. E., Revill A. T., Smith C. I., Komugabe A. F. and Fallon S. F.
977 (2014) Preservation effects on the isotopic and elemental composition of skeletal
978 structures in the deep-sea bamboo coral Lepidisis spp. (Isididae). *Deep-Sea Research*
979 *Part II: Topical Studies in Oceanography* **99**, 199–206.
980 Stuiver M., Reimer P.J. and Reimer R. W. (2021) CALIB 8.2 http://calib.org (accessed Feb-7-
981 2021).
982 Sun X. and Turchyn A. V. (2014) Significant contribution of authigenic carbonate to marine
983 carbon burial. *Nature Geoscience* **8**, 1–4.
984 Tesdal J. E., Galbraith E. D. and Kienast M. (2013) Nitrogen isotopes in bulk marine sediment:
985 Linking seafloor observations with subseafloor records. *Biogeosciences* **10**, 101–118.
986 Williams B. (2020). Proteinaceous corals as proxy archives of paleo-environmental change.
987 *Earth-Science Reviews **209***, 103326.
988 Williams B. and Grottoli A. G. (2010) Recent shoaling of the nutricline and thermocline in the
989 western tropical Pacific. *Geophysical Research Letters* **37**, 2–6.
990 Yamashita Y. and Tanoue E. (2003) Distribution and alteration of amino acids in bulk DOM
991 along a transect from bay to oceanic waters. *Marine Chemistry* **82**, 145-160.
992 Zaiontz C. (2019) Real Statistics Resource Pack software (Release 6.2). Copyright (2013 – 2019)
993 www.real-statistics.com
994

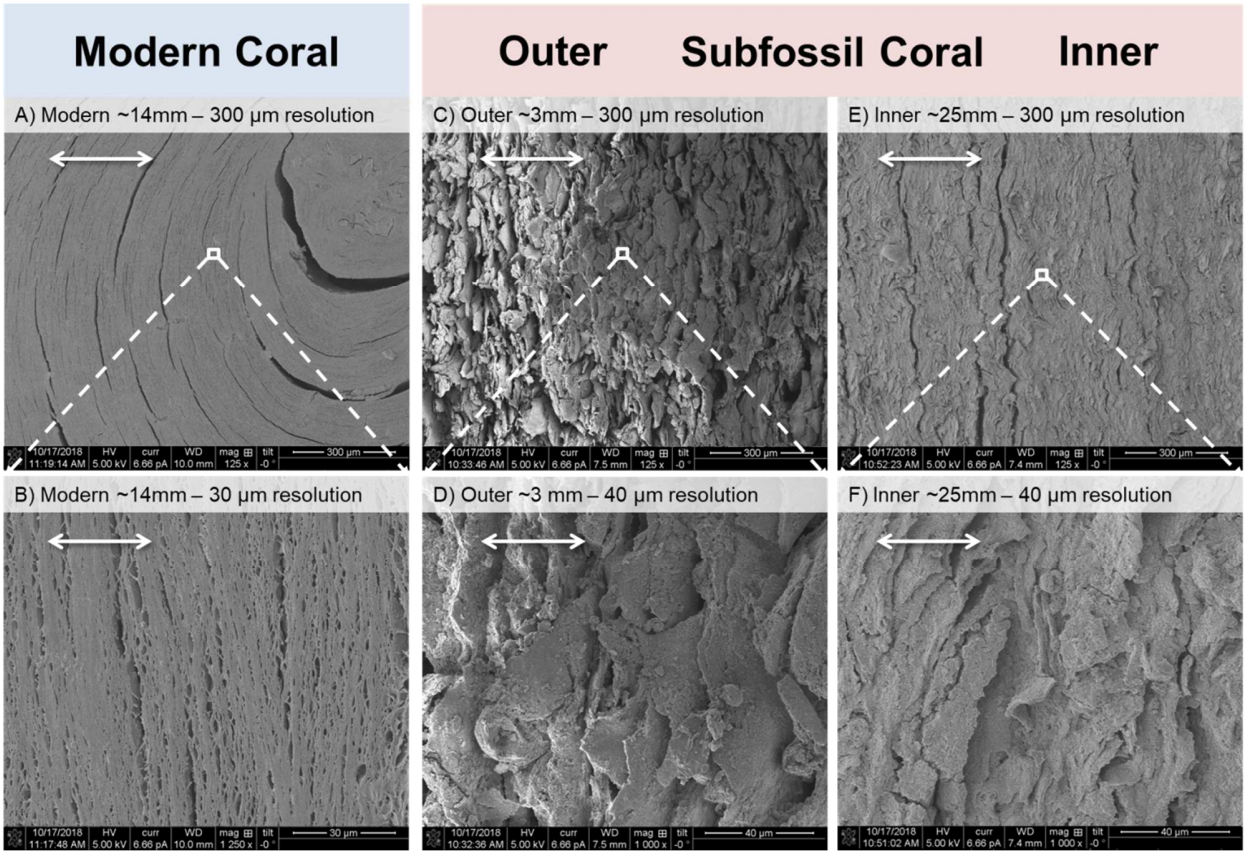

Fig. 1) Scanning electron microscope (SEM) images live-collected *Kulumanamana haumaaea* and subfossil gold coral skeletons collected from the same Cross Seamount location. For all figures, the growth axis progresses from right to left (outer layers left, inner layers right). Images on the top are magnified by 125x while the bottom are higher magnifications and representing the area inside the red squares on top images; scale bars are white arrows and also on lower right of each image. **A and B)** Live-collected coral skeletons showing the layered fibrous nature of living skeletons from ~14 mm from edge. Panel B is a 1250x (30 µm) magnified image of the modern of area in the white square; ~600 yr CE). **C and D)** Outer subfossil coral material, ~3 mm from the outer edge (~9.6 kyrs BP), which shows extreme structural alteration at 1000x (40 µm) magnification. **E and F)** Inner subfossil coral material imaged ~25 mm from the edge (~10.7 kyr BP), with similar magnifications to the outer layers.

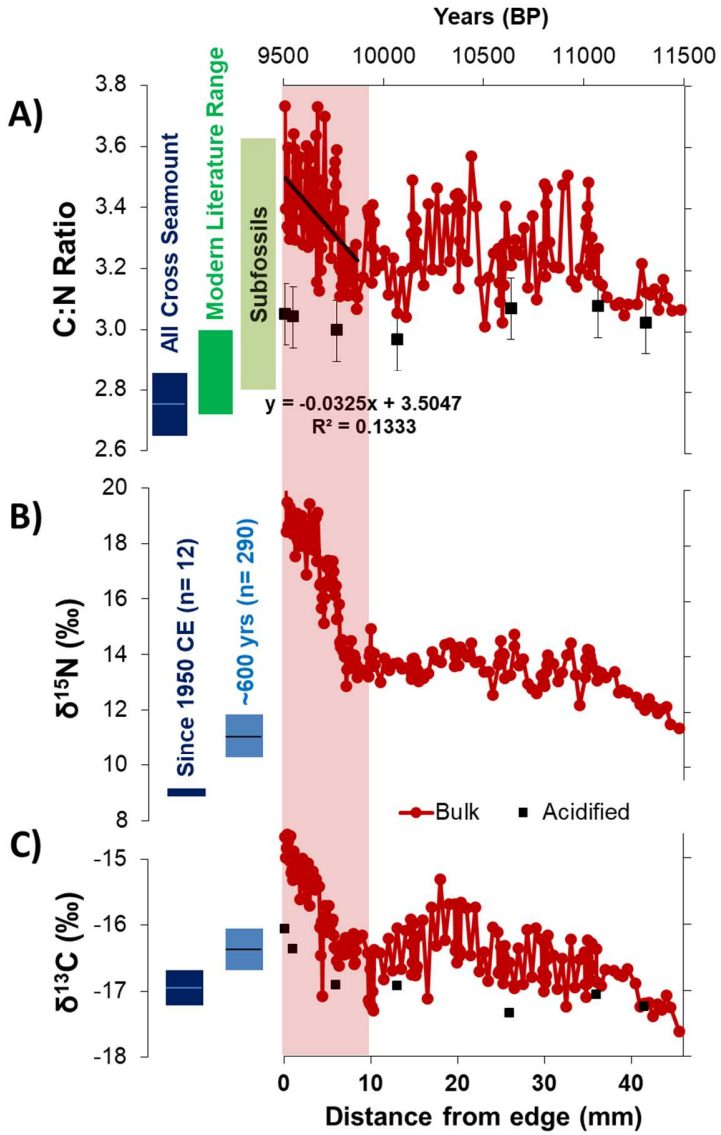

Fig. 2) C/N and bulk isotope values. **A)** C/N ratios for *K. haumaeea* coral skeletons. From left to right, a live-collected Cross Seamount coral C/N average and standard deviation (blue, this study), literature range for live-collected corals (dark green; Druffel et al., 1995, Goodfriend 1997; Sherwood et al., 2014; McMahon et al., 2015), range of previous dead-collected, subfossil coral values (light green; 1-5 kyrs BP, Glynn et al., 2019), and this study's results for a subfossil Cross Seamount skeleton (red). **B)** Bulk nitrogen and **C)** bulk carbon isotope values of live-collected (blue boxes) and subfossil *K. haumaeea* (red) gorgonin skeletal material, collected from the same Cross Seamount site. Due to the rapid change in isotopic values during the Industrial Revolution, live-collected coral values are plotted as separate averages and standard deviations for recent time (dark blue, since 1950 CE) versus the pre-Industrial Revolution (before 1900 CE, ~600 yrs). The subfossil coral data represents a 46 mm transect from the outer layers to the inner layers, with each point representing 0.1 mm resolution (~5-7 yrs). Black

squares are for selected acidified samples. Pink shading represents the outer 10 mm diagenetic horizon discussed in the text.

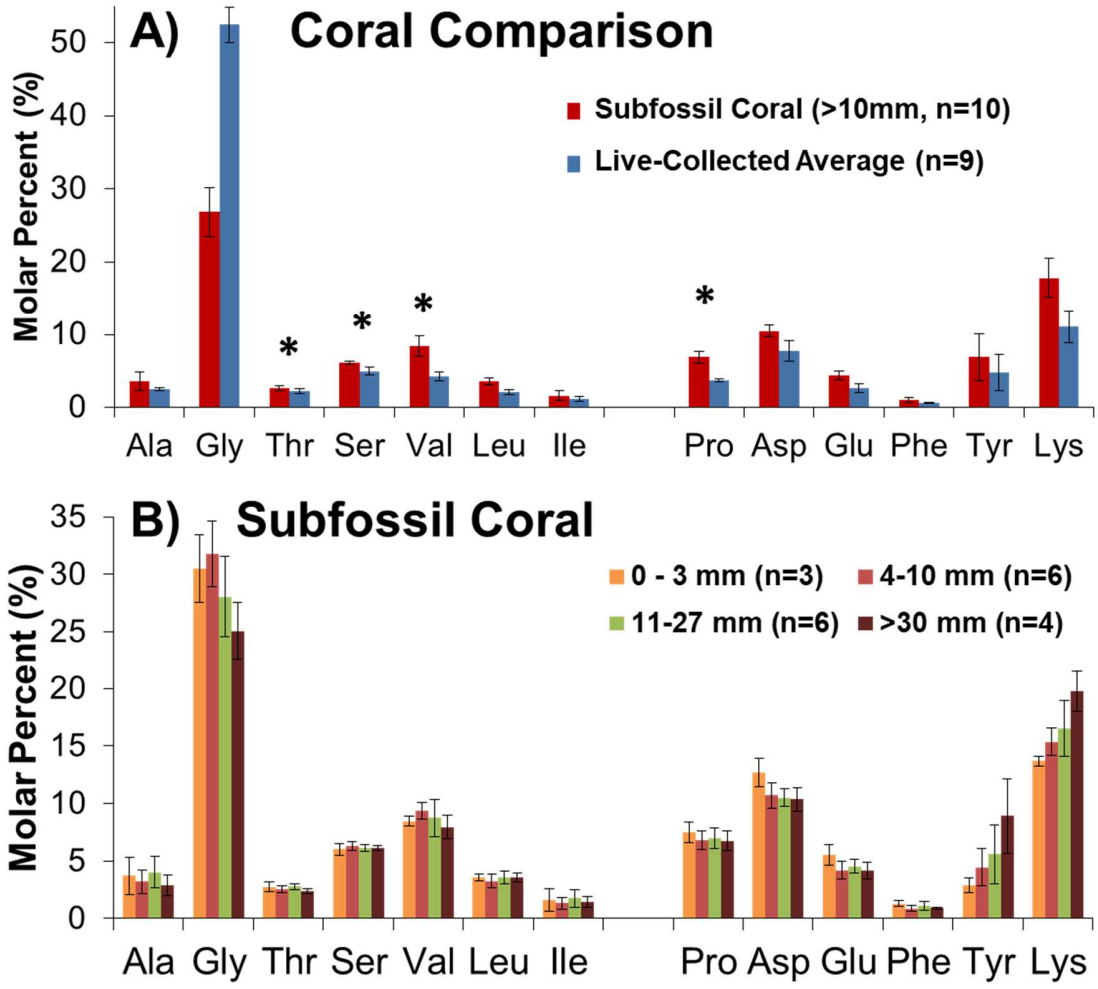

Fig. 3) Molar percentage (mol%$_{AA}$) of AAs for ancient and modern *K. haumaeea* skeletons. **A)** Subfossil vs. Modern *K. haumaeea* mol%$_{AA}$ comparison. Average molar distribution in modern specimen (n=9; blue bars) versus average of only subfossil coral inner layers (>10 mm, n=10, red bars). There were significant mol%$_{AA}$ differences between all AAs ($P < 0.02$) except Tyr ($P < 0.12$) and Ile ($P < 0.09$; t-test assuming unequal variances, alpha = 0.05). AA's denoted with a star (*) indicate AA's which retain significantly different mol%$_{AA}$ values if Gly values are set to be equal, as described in the text. **B)** Inter-coral subfossil skeleton mol%$_{AA}$ data (n=19) from Cross Seamount, HI. Data are binned by skeletal depth highlighting AA composition changes between degraded outer layers vs. protected inner layers.

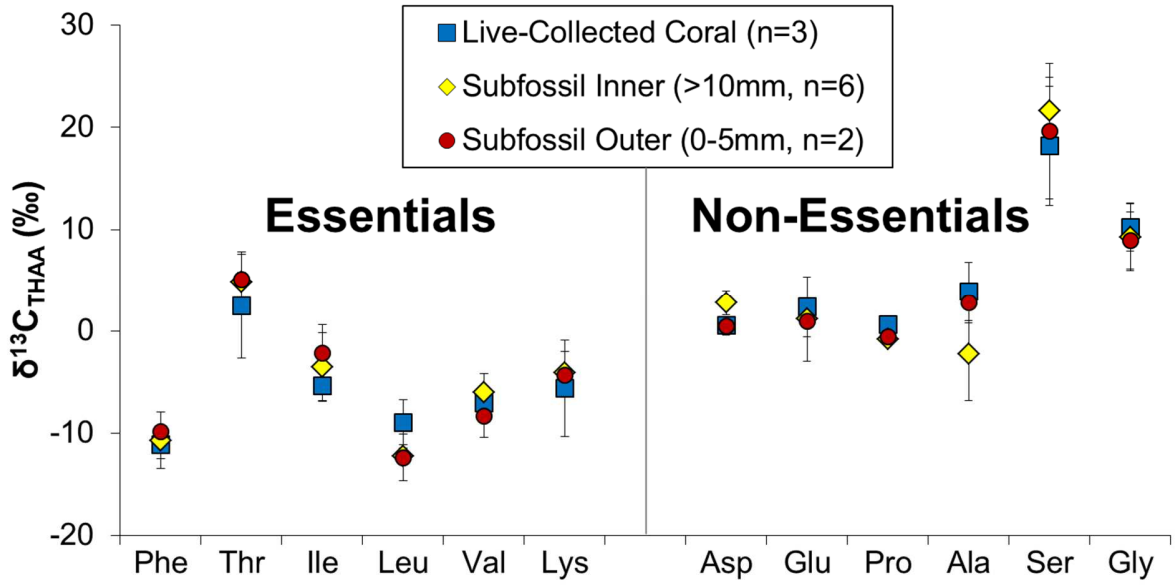

Fig. 4) Normalized $\delta^{13}C$ AA values in live-collected (blue) and subfossil *K. haumaeea* skeletons (red and yellow). AA $\delta^{13}C$ values normalized by subtraction of average THAA ($\delta^{13}C_{THAA}$). AAs are grouped as described in the text and error bars indicate the standard deviation of the average binned $\delta^{13}C$ values.

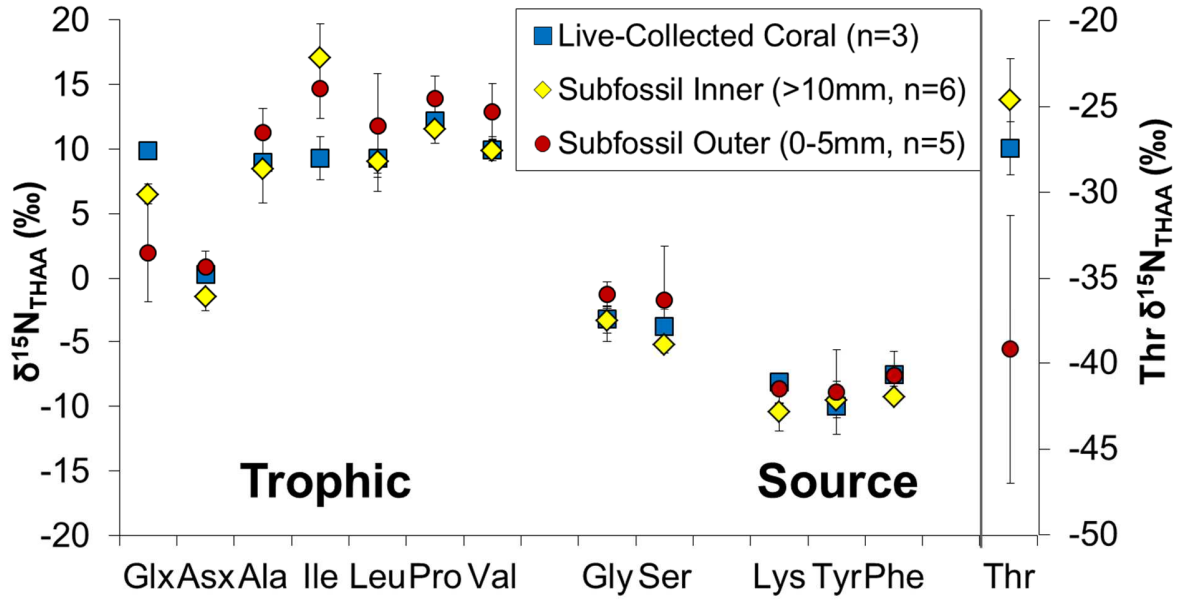

Fig. 5) Normalized $\delta^{15}N$ isotope values for AAs of the live-collected (blue) and subfossil *K. haumaeea* skeletons (red and yellow). AA $\delta^{15}N$ values normalized by subtraction to average $\delta^{15}N$ of hydrolysable protein (THAA parameter; see methods). Note that Thr is plotted on a separate secondary axis. AAs are grouped as described in the text and error bars indicate the standard deviation of the binned coral values.

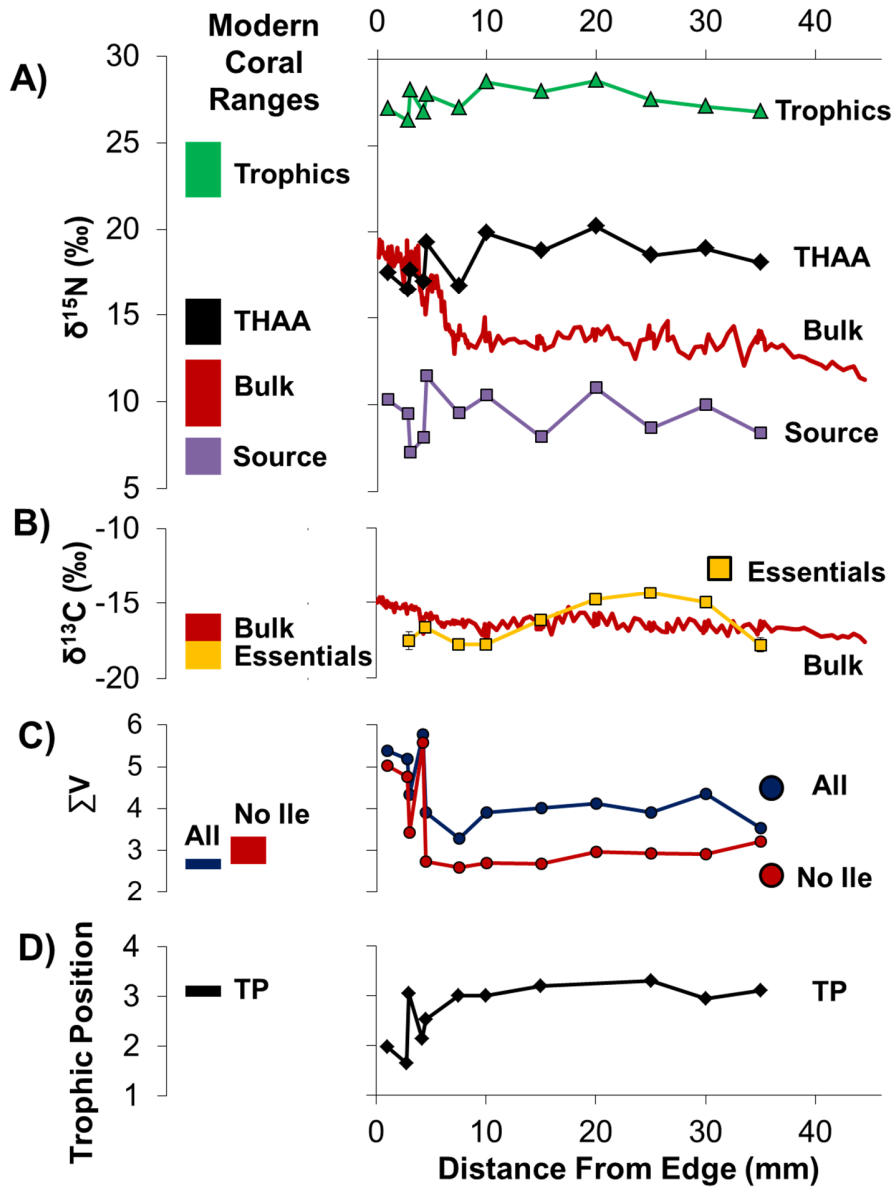

Fig. 6) Modern coral ranges compared to subfossil coral $\delta^{15}N_{AA}$ proxies. Ranges of values found for the modern specimen on the left and the subfossil coral on the right. **A)** Bulk $\delta^{15}N$ values plotted along with average total hydrolysable AAs (THAA) $\delta^{15}N$ average values (black), average $\delta^{15}N$ value of the trophic AAs (Glx, Asx, Ala, Ile, Leu, Pro, Val), and average $\delta^{15}N$ values source AA values (Phe, Lys, Tyr). **B)** Average of measured $\delta^{13}C$ values for essential AA (Phe, Thr, Ile, Leu, Val, Lys) plotted along with the bulk $\delta^{13}C$ values. **C)** $\sum V$ values, calculated using all trophic AAs (blue) and excluding Ile values (red). **D)** Trophic position after McMahon et al. 2018 (see methods).